Mutation in *Bmpr1b* Leads to Optic Disc Coloboma and Ventral Retinal Gliosis in Mice

Xiaohe Yan,[1,2] Jenny Atorf,[3] David Ramos,[4] Frank Thiele,[5] Susanne Weber,[6] Claudia Dalke,[6,7] Minxuan Sun,[6,7] Oliver Puk,[6,7] Dian Michel,[5] Helmut Fuchs,[5,7] Matthias Klaften,[5] Gerhard K.H. Przemeck,[5] Sibylle Sabrautzki,[5] Jack Favor,[7,8] Jesús Ruberte,[4] Jan Kremers,[3] Martin Hrabě de Angelis,[5,7,9,10] and Jochen Graw[6,7]; German Mouse Clinic Consortium

[1]Shenzhen Key Laboratory of Ophthalmology, Shenzhen Eye Hospital, Jinan University, Shenzhen, China
[2]School of Optometry, Shenzhen University, Shenzhen, China
[3]Department of Ophthalmology, University Hospital Erlangen, Erlangen, Germany
[4]Department of Animal Health and Anatomy, Center of Animal Biotechnology and Gene Therapy, Universitat Autònoma de Barcelona, Barcelona, Spain
[5]Institute of Experimental Genetics, Helmholtz Zentrum München, Neuherberg, Germany
[6]Institute of Developmental Genetics, Helmholtz Zentrum München, Neuherberg, Germany
[7]The German Mouse Clinic, Helmholtz Zentrum München, Neuherberg, Germany
[8]Institute of Human Genetics, Helmholtz Zentrum München, Neuherberg, Germany
[9]Chair of Experimental Genetics, Faculty of Life and Food Sciences Weihenstephan, Technische Universität München, Freising-Weihenstephan, Germany
[10]German Center for Diabetes Research (DZD), Neuherberg, Germany

Correspondence: Xiaohe Yan, Shenzhen Key Laboratory of Ophthalmology, Shenzhen Eye Hospital, Jinan University, School of Optometry, Shenzhen University, Zetian Road 18, 518040 Shenzhen, Guangdong, China; yanxh1@hotmail.com.

A full list of consortium members appears in the Supplementary materials.

Current affiliations: JA: Municipal Eye Hospital, Karlsruhe, Germany.
DR: CIISA–Centre for Interdisciplinary Research in Animal Health, Faculty of Veterinary Medicine, Universidade de Lisboa, Lisbon, Portugal.
FT: Institute of Virology, Helmholtz Zentrum München, München, and Institute of Virology, Technical University Munich, München, Germany.
CD: Institute of Metabolism and Cell Death, Helmholtz Zentrum München, Neuherberg, Germany.
MS: Jiangsu Key Lab of Medical Optics, Suzhou Institute of Biomedical Engineering and Technology, Chinese Academy of Sciences, Suzhou, China.
OP: Practice of Human Genetics, Tübingen, Germany.
DM: Deutsches Zentrum für Luft- und Raumfahrt e. V. (DLR), DLR Project Management Agency, Bonn, Germany.
MK: Amcure GmbH, Eggenstein-Leopoldshafen, Germany.

Purpose. The clinical phenotype of retinal gliosis occurs in different forms; here, we characterize one novel genetic feature, (i.e., signaling via BMP-receptor 1b).

Methods. Mouse mutants were generated within a recessive ENU mutagenesis screen; the underlying mutation was identified by linkage analysis and Sanger sequencing. The eye phenotype was characterized by fundoscopy, optical coherence tomography, optokinetic drum, electroretinography, and visual evoked potentials, by histology, immunohistology, and electron-microscopy.

Results. The mutation affects intron 10 of the *Bmpr1b* gene, which is causative for skipping of exon 10. The expression levels of pSMAD1/5/8 were reduced in the mutant retina. The loss of BMPR1B-mediated signaling leads to optic nerve coloboma, gliosis in the optic nerve head and ventral retina, defective optic nerve axons, and irregular retinal vessels. The ventral retinal gliosis is proliferative and hypertrophic, which is concomitant with neuronal delamination and the reduction of retinal ganglion cells (RGCs); it is dominated by activated astrocytes overexpressing PAX2 and SOX2 but not PAX6, indicating that they may retain properties of gliogenic precursor cells. The expression pattern of PAX2 in the optic nerve head and ventral retina is altered during embryonic development. These events finally result in reduced electrical transmission of the retina and optic nerve and significantly reduced visual acuity.

Conclusions. Our study demonstrates that BMPR1B is necessary for the development of the optic nerve and ventral retina. This study could also indicate a new mechanism in the formation of retinal gliosis; it opens new routes for its treatment eventually preventing scar formation in the retina.

Keywords: Bmpr1b, mouse model, retinal gliosis, optic nerve coloboma

iovs.arvojournals.org | ISSN: 1552-5783

Investigative Ophthalmology & Visual Science

SS: Research Unit Comparative Medicine, Helmholtz Zentrum München, Neuherberg, Germany.
JF, JG: Retired.

Received: November 23, 2018
Accepted: November 10, 2019
Published: February 27, 2020

Citation: Yan X, Atorf J, Ramos D, et al. Mutation in *Bmpr1b* leads to optic disc coloboma and ventral retinal gliosis in mice. *Invest Ophthalmol Vis Sci.* 2020;61(2):44. https://doi.org/10.1167/iovs.61.2.44

Bone morphogenetic protein (BMP) signaling plays an essential role in eye development. Mutations in *BMP4* cause anophthalmia (no eyes) or microphthalmia (small eyes) and developmental anomalies in human limbs.[1] BMP4 is essential for lens induction during early eye development in the mouse[2]; it also plays a fundamental role in the dorsoventral polarity of the eye cup and controls cell apoptosis in the developing eyes.[3,4] However, knockdown of *Bmp4* does not produce discernable retinal phenotypes.[5] In human patients, mutations in *BMP4* cause anophthalmia-microphthalmia and retinal dystrophy.[6] Moreover, *Bmp7* knockout mice exhibit microphthalmia or anophthalmia caused by disruptions of lens induction during early eye development.[7–9] However, loss of *Bmp7* causes eye defects that are variable and strain specific.[7–10] In the retina, *Bmp4* is expressed in the dorsal portion and *Bmp7* is expressed in the distal periphery. However, the corresponding Bmp type I receptors are found mainly in the ventral retina during eye development.[11,12]

BMP signaling occurs through its receptors BMPR1A, BMPR1B, or BMPR2. They form a family of transmembrane kinases, which consist of an *N*-terminal signal sequence, an extracellular ligand-binding domain, a transmembrane domain, and a cytoplasmic serine/threonine kinase. Here, we focus on the *Bmpr1b* gene, which is highly conserved between humans and mice. Patients with *BMPR1B* mutations are mainly characterized by brachydactyly (a shortness of the fingers and toes) or chondrodysplasia (skeletal dysplasia) (OMIM 603248). Similarly, *Bmpr1b* mutations in the mouse affect the shape of the distal limb skeleton, resulting in brachydactyly. Moreover, BMPR1B is expressed during the early stages of eye development in the optic vesicle (at E9.0–E9.5), the ventral retina (at E10.5–E11.5),[11] retinal progenitor cells (at E14.5), and in later stages retinal ganglion cells.[13] In homozygous *Bmpr1b* knockout mice, retinal axons are misguided in the optic nerve head at E15.5 to E16.5.[14] Interestingly, conditional *Bmpr1a* knockout mice (lacking retinal *Bmpr1a* function in the *Six3-Cre* transgenic background) have normal eye development, whereas *Bmpr1a/Bmpr1b* double knockout mice show severe retinal defects, including retinal growth and neurogenesis,[15] suggesting that BMPR1B may play a more important role in retinal development.

However, very few studies have investigated the role of BMP signaling in the retina. It was reported that BMP7 regulates reactive gliosis in retinal astrocytes and Müller cells in vitro.[16] In the present study, we characterized a new *Bmpr1b* mouse mutant line generated within a genome-wide recessive *N*-ethyl-*N*-nitrosourea (ENU) mutagenesis screen.[17] The mutation leads to a skipping of exon 10 of *Bmpr1b* and results in optic nerve coloboma with gliosis of the optic nerve head and of the ventral retina, which is associated with abnormal retinal vessels. Visual acuity is significantly reduced in the homozygous mutants, and electrophysiologic transmission of the retina and optic nerve is affected. Moreover, we showed that the ventral proliferative and hypertrophic retinal gliosis induced by the *Bmpr1b* mutation is dominated by astrocytes expressing markers of progenitor cells. This ocular phenotype was not observed in the *Bmpr1b*-knockout mouse.[14] Therefore, our new and rather neomorphic allele of *Bmpr1b* demonstrates that retinal BMP signaling acts via BMPR1B, at least in mice. Moreover, this function might open new routes for therapeutic approaches to prevent gliosis and eventual scar formation.

Materials and Methods

Mice

Mice were kept under specific pathogen-free conditions at the Helmholtz Center Munich. The use of animals was in accordance with the German Law of Animal Protection and the tenets of the Declaration of Helsinki. Male C3HeB/FeJ mice were treated with ENU (80 mg/kg body weight applied by intraperitoneal injection in three weekly intervals) at the age of 10–12 weeks as previously described[18,19] and mated to untreated female C3HeB/FeJ mice.[17] The offspring of the ENU-treated mice were screened at the age of 11 weeks for general dysmorphology features[20]; this part of the experiments was performed with permission of the district government of Upper Bavaria as the local Animal Welfare Authority (55.2-1-54-2432-126-11). For detailed analysis of the ocular phenotype, including the retina and the optic nerve, and electrophysiologic analysis, the mutation was also bred on the C57BL/6J background. The electroretinogram (ERG) and visual evoked potential (VEP) studies were performed with permission of the district government of Middle Franconia as the local Animal Welfare Authority (54-2532.1-23/12).

Linkage Analysis

Homozygous carriers (first generation) were mated to wild-type C57BL/6J mice, and the offspring (second generation) was intercrossed. DNA was prepared from tail tips of affected offspring of the third generation (G3). For linkage analysis, genotyping of a genome-wide mapping panel consisting of 153 single-nucleotide polymorphisms (SNPs) was performed using MassExtend, a matrix-assisted laser/desorption ionization–time of flight mass spectrometry

TABLE. Primers

Primer	Sequence (5′→3′)	Annealing Temperature (°C)	Product Size (bp)
Exon10-L	GAGGAAATTTGCATGTTAGGC	55	302
Exon10-R	GCCACCTCAAAATGAGTTTC		
Exon8fw	TAGACGCAAAGTCCATGCTG	58	See below
Exon9fw	GCGCTATATGCCTCCAGAAG		
Bmpr1bSplicervE11	TGACATTTTGGCAAGGGTTT		

Product sizes: Exon8fw + Bmpr1bSplicervE11: wt: 599 bp; mutant: 468 bp. Exon9fw + Bmpr1bSplicervE11: wt: 361 bp; mutant: 230 bp.

high-throughput genotyping system supplied by Sequenom (San Diego, CA, USA).[21]

Genotyping, Cloning, and Sequencing

Genomic DNA was isolated from tail tips of C57BL/6J and C3HeB/FeJ wild-type mice or homozygous/heterozygous mutants according to standard procedures; complementary DNA (cDNA) was isolated from the entire eye or from the retina; the primers for the corresponding polymerase chain reactions (PCRs) of the *Bmpr1b* cDNA are given in the Table. PCR was performed with a PTC-225 thermocycler (Biozym, Hessisch Oldendorf, Germany). Products were analyzed by electrophoresis on a 1.5% agarose gel. Sequencing was performed at GATC Biotech (Konstanz, Germany) or at the Helmholtz Center Munich using an ABI 3100 sequencer (Applied Biosystems, Darmstadt, Germany).

Comprehensive Phenotyping in the German Mouse Clinic

Comprehensive phenotyping of 20 male and 20 female homozygous *Bmpr1b* mutant mice and the corresponding wild-type littermates was performed at the German Mouse Clinic (http://www.mouseclinic.de) using a standard battery of tests.[20,22,23] Since some tests have been performed in parallel, the number of mice used in the individual tests might be smaller than the total number mentioned above. If not otherwise stated, data of males and females were analyzed separately using Student's *t*-test or analysis of variance.

Spectral Domain Optical Coherence Tomography (SD-OCT) Imaging

SD-OCT was used to acquire retinal images. The mice were anesthetized with an intraperitoneal injection of 137 mg ketamine and 6.6 mg xylazine per kilogram of body weight and the pupils were dilated with 1% atropine. Then the mouse eyes were covered with lens glass to neutralize the refractive power of the cornea and make the optical coherence tomography (OCT) beam focus on the retina.[24] OCT images were recorded with the equipment set to 30° field of view. Horizontal or vertical consecutive images were made in the center of the optic nerve head. To improve the signal-to-noise ratio, the images were averaged using the built-in functions in the system.

Visual Acuity Measurements by Optokinetic Drum

Vision tests were performed between 9 AM and 4 PM using a virtual optomotor system (Cerebral Mechanics, Lethbridge, Canada) as described previously.[25] Briefly, a rotating cylinder covered with a vertical sine wave grating was calculated and drawn in virtual three-dimensional space on four computer monitors arranged in a square. Visually unimpaired mice tracked the grating with reflexive head and neck movements (head-tracking). Vision threshold of the tested mice was quantified by a simple staircase test. Rotation speed and contrast were set to 12.0 d/s and 100%, respectively. Since no significant threshold differences were observed between males and females ($P > 0.05$; *t*-test), data of both sexes were combined. Thresholds of wild-type, heterozygous, and homozygous *ALI030* mice (C57BL/6J background, age: 10 weeks) were compared using a linear mixed-effect model for grouped data (R package).

ERGs and VEPs

ERGs and VEPs were measured simultaneously in 14 C57BL/6J control mice and 9 heterozygous and 9 homozygous mutant mice. One week prior to the measurements, a small nickel screw (M2 × 6 mm; RS Components Pte Ltd, Singapore, Singapore), which later served as the active electrode for measuring the VEPs, was implanted onto the skull above the right superior colliculus, the part of the mouse brain where visual information is processed. For this surgery, the skin over the skull of the anesthetized mice (50 mg/kg ketamine [Ketavet; Pfizer, Berlin, Germany] and 10 mg/kg xylazine [Rompun 2%; Bayer, Leverkusen, Germany]) was opened and additional local anesthesia was administered (Xylocain; AstraZeneca GmbH, Wedel, Germany). A small trepanation was performed using a veterinary dental drill. The screw was inserted into the right visual cortex (1.5 mm lateral to the midline, 1.5 mm anterior to lambda) as previously described.[26] Before suturing the skin, the wound area was kept aseptic with octenidine dihydrochloride (Octenisept; Schülke & Mayr GmbH, Norderstedt, Germany).

A detailed description of measuring standard scotopic and photopic ERGs can be found elsewhere.[27–29] Briefly, dark-adapted mice (overnight) were anesthetized (50 mg/kg ketamine [Ketavet] and 10 mg/kg xylazine [Rompun 2%]), and a subcutaneous injection of saline solution (10 mL/kg, 0.9%) protected the mice from desiccation. The pupils were dilated with a drop of tropicamide (Mydriaticum Stulln, 5 mg/mL; Pharma Stulln GmbH, Stulln, Germany) and phenylephrin-hydrochloride (Neosynephrin POS 5%; Ursapharm, Saarbrücken, Germany). To measure the ERGs from the left eye, a ground needle electrode was placed subcutaneously at the base of the tail, a reference needle electrode was positioned subcutaneously next to the left ear, and the active contact lens electrode (Mayo Corporation, Inazawa, Japan), internally covered with Corneregel (Dr. Mann Pharma, Berlin, Germany), was placed on the cornea of the left eye (i.e., contralateral to the VEP electrode, thereby ensuring that the ERGs were recorded from the eye

Investigative Ophthalmology & Visual Science

that provided the main input for the measured VEPs). For simultaneous measurement of the VEPs, the implanted screw was connected to the amplifier as the active electrode, and the reference needle electrode was placed subcutaneously next to the right ear.

To deliver the stimuli, a Ganzfeld Bowl (Q450 SC; Roland Consult, Brandenburg, Germany) was used. Stimulation and data recording were controlled using a RetiPort system (Roland Consult). Initially, dark-adapted flash (between a 5-µs and 5-ms duration) ERGs and VEPs were measured. The flash strength was increased in eight steps (0.0002, 0.002, 0.0063, 0.02, 0.063, 0.2, 0.63, and 6.3 cd·s/m^2), and depending on the flash strength, 8 to 12 flash responses were averaged. After 5 minutes of adaptation to a 25-cd/m^2 steady background light, photopic flash ERG and VEP measurements were performed. Flashes of five strengths (0.063, 0.2, 0.63, 2, and 6.3 cd·s/m^2) were superimposed onto the background. At each flash strength, 20 responses were averaged. ERG and VEP signals were amplified 100,000 times, bandpass filtered between 1 and 300 Hz, and digitized with a sampling frequency of 2048 Hz.

For the flash ERGs, the amplitudes and delays of the a- and b-waves as well as the amplitudes of the oscillatory potentials were determined. The amplitude of the a-wave was defined as the difference between baseline (average voltage of the 30 ms prior to stimulation) and the trough of the a-wave in a window between 30 and 90 ms after stimulation. The amplitude of the b-wave was defined as the potential difference between the trough of the a-wave and the peak of the b-wave in a time window between 55 and 150 ms poststimulation. In addition, the amplitudes and delays of the N1 (first negative trough) and the P1 and P2 (first and second positive peaks) components of the scotopic and photopic flash VEPs were measured. The N1 amplitude was defined as the difference between the baseline before stimulation and the trough of N1, and the amplitudes of P1 and P2 were measured as the difference between the N1 trough and the P1 or P2 peak, respectively.

Statistical analysis was performed with SYSTAT 13 (Systat Software, Inc., Chicago, IL, USA) using the Kruskal-Wallis test. Note that statistically significant differences ($P < 0.05$) were determined only for the signals obtained at the highest flash strength of 6.3 cd·s/m^2, because the responses at other strengths cannot be considered independent.

Histology and Electron Microscopy

Mouse eyes from postnatal stages were analyzed histologically for eye pathologies. Tissues were fixed in Davidson solution and embedded in JB-4 plastic medium (Polyscience, Inc., Eppelheim, Germany) according to the manufacturer's protocol. Sectioning was performed with an ultramicrotome (OMU3; Reichert-Jung, Walldorf, Germany). Serial transverse 3-µm sections were cut with a glass knife and stained with methylene blue and basic fuchsin. The sections were evaluated with a light microscope (Axioplan; Carl Zeiss, Jena, Germany). Images were acquired by means of a scanning camera (AxioCam; Jenoptik, Jena, Germany).

For transmission electron microscopic analysis, retinal fragments were fixed in 2.5% glutaraldehyde and 2% paraformaldehyde, postfixed in 1% osmium tetroxide, stained in aqueous uranyl acetate, dehydrated, and embedded in epoxy resin. Ultrathin sections (70 nm) were stained using lead citrate and examined by a transmission electron microscope (Hitachi H-7000; Hitachi, Tokyo, Japan).

The cross sections (2–3 µm) of the optic nerve were immersed in 1% toluidine blue solution and dried on a hot plate for 1 minute, followed by washing them with tap water. The slides were mounted with EUKITT quick-hardening mounting medium (Sigma-Aldrich Chemie GmbH, Munich, Germany). The number of total axons was counted using ImageJ software (National Institutes of Health, Bethesda, MD, USA).

Anterograde Tracing

E15.5 embryos were fixed in 4% PFA (paraformaldehyde) in phosphate-buffered saline (PBS) overnight, and the cornea was incised by forceps, the lens was removed, and the optic cup was packed with lipophilic tracers DiI (red) or DiO (green) (Invitrogen, Thermo Fisher Scientific, Waltham, USA) DiI or DiO. The lens was replaced in the eye and the cornea was covered. The embryos were refixed in 4% PFA in PBS for approximately 1 month at room temperature to allow the tracers to diffuse along axons completely. The optic nerve, optic chiasm, and optic tract were exposed after removing the heads and analyzed by stereo-fluorescence microscopy.

Immunohistochemistry and Confocal Microscopy

For immunohistochemistry, embryonic eyes or postnatal retina were fixed in 4% PFA at 4°C from 2 hours to overnight (depending on the size of embryonic tissues) or 20 minutes (retina) and then transferred to 30% sucrose for cryosection and embedded in OCT Compound Tissue Tek (Sakura Finetek Germany GmbH, Staufen, Germany) and stored at –80°C. Sections (12 µm) were cut on a cryostate (CM1950; Leica Microsystems CMS, Wetzlar, Germany). For the study of adult whole-mount retinas, the retinas were fixed in 4% PFA for 20 minutes and then washed in PBS/0.1%Triton X-100 two times and penetrated in 0.1 M glycin/PBS. The retinas were incubated in primary antibodies or blocking solution (control) for overnight. After washing in phosphate buffered saline with 0.1% TritonX-100 (PBST), the embryos were incubated with secondary antibodies for 24 hours, followed by staining in 4′,6-diamidino-2-phenylindole (DAPI) (1:10,000) for 20 minutes. The embryos were preserved and imaged in 80% glycerol and the Poly-Mount mounting medium (Polysciences Europe GmbH, Hirschberg an der Bergstraße, Germany).

Primary antibodies (Supplementary Table S2a) were used for incubation at 4°C overnight, followed by a secondary antibody with fluorescence against the species of the primary antibody at room temperature for 1 to 1.5 hours (antibody list in Supplementary Table S2b). For 5-bromo-2-deoxyuridine (BrdU) labeling, 2N HCl was used to expose the nuclear antigen for 20 minutes at 37°C. Counterstaining of the cell nuclei was performed with DAPI (Sigma-Aldrich Chemie GmbH, Munich, Germany; dilution 1:10,000). The immunofluorescence pictures were taken by confocal microscopy (Olympus, Hamburg, Germany, and Leica Microsystems, Mannheim, Germany). The images were analyzed by a FluoView 1.7 software (Olympus, Tokyo, Japan).

BrdU Labeling

The thymidine analogue, BrdU, incorporates into newly synthesized DNA during the S-phase of the cells. It is used to label proliferating cells in mice.[30] To investigate the prolif-

eration of ventral glial cells in postnatal *ALI030* mice (P21), BrdU was injected intraperitoneally (0.05 mg/g, dissolved in 0.09% NaCl solution) and the mice were killed at 24 hours after injection.

Western Blot

Briefly, 3-week mouse eye balls were enucleated and retinas were isolated. The protein concentration was determined by a BCA protein assay kit (Pierce, Rockford, IL, USA). The retinal protein samples were adjusted to the same amount (20 µg). The loading buffer (4×) was added into the samples and incubated at 95°C for 10 minutes. The samples were loaded on the gel and the proteins were first transferred to a polyvinylidene fluoride (PVDF) membrane in a transfer chamber by electrophoresis. The PVDF membranes were blocked in 5% milk power in TBST for 30 minutes at room temperature. Then the membranes were incubated with primary antibody (pSMAD1/5/8 1:1000, AB3848-I, Millipore, Temecula, USA; SMAD1/5/8 1:1000, 21684, SAB, Baltimore, USA; GAPDH 1:2500, G9545, Sigma-Aldrich, St. Louis, US) at 4°C overnight. The horseradish peroxidase (HRP)–conjugated secondary antibodies (IgG/HRP, 1:5000, AS038; ABclonal, Woburn, MA, USA) were incubated for 45 minutes at room temperature on the PVDF membrane. The HRP from secondary antibody was detected by adding chemiluminescence detection reagent (Immobilon Western Chemiluminescent HRP Substrate, Cat. No. WBKLS0010; Millipore) on the membrane and was visualized using ChemiDoc XRS system (Bio-Rad, Hercules, CA, USA).

General

Chemicals and enzymes were obtained from Fermentas (St-Leon-Rot, Germany), Merck (Darmstadt, Germany), or Sigma Chemicals (Deisenhofen, Germany). Oligonucleotides were synthesized by Sigma Genosys (Steinheim, Germany).

Results

Detection of the *ALI030* Mutants and Identification of the Underlying Mutation

The recessive *ALI030* mouse line (this *Bmpr1b* mutant mouse line was referred to as abnormal limb #030 (*ALI030*) according to the internal lab code, see Supplementary Materials) was generated within our large-scale genome-wide ENU mutagenesis screen for recessive mutants. The mutation was mapped to mouse chromosome 3 between the SNP markers rs13477421 and rs13477460 (109–143 Mb, chromosome 3, mouse genome Build 37.1); haplotype analysis using microsatellites reduced the critical interval (130–140 Mb). After mapping and sequencing of candidate genes, the mutation could be annotated to the second base in intron 10 of the *Bmpr1b* gene (T→G) (Fig. 1a). The mutation does not change a restriction site, which could be used experimentally; therefore, genotyping of mutants was performed by sequencing a 440-bp fragment amplified from genomic DNA.

Since the mutation affects the splice donor site of exon 10, we tested the hypothesis that the mutation affects splicing. cDNA from wild-type and homozygous *ALI030* mice was analyzed by PCR covering the critical region (exon 10) using primers for amplification of either exons 8 to 11 or exons 9 to 11. As shown in Figure 1b, we observed shorter (131-bp) PCR amplicons in mutant mice referring to a mutation-related splice defect in *ALI030*. Sequence analysis confirmed that exon 10 is completely spliced out in homozygous mutants (Supplementary Fig. S1) leading to a direct connection of exon 9 and exon 11; a schematic representation of the altered splice event is depicted in Figure 1c. Since this alternative splicing leads to a frame shift, 26 new amino acids are predicted in front of a premature stop codon. The *N*-terminal signal peptide, the ligand-binding domain, and the transmembrane domain are not affected; however, the C-terminal part of the protein-kinase domain, including its active site in the cytoplasm, is suggested to be destroyed.

Eye phenotype screening was performed at the German Mouse Clinic; homozygous mutant mice had severe ocular defects as demonstrated by an enlarged optic disc on the C3HeB/FeJ (C3H) background (supplementary materials; Supplementary Fig. S2); homozygous mutants backcrossed to the C57BL/6J background were not able to react to the moving stripes in the virtual drum, suggesting poor vision (Fig. 1d). Slightly enlarged eye axial lengths were found in the mutants (supplementary materials; Supplementary Table S1). The rest of experiments of the *ALI030* mouse were performed on the C57BL/6J background. The ocular pathology was restricted to the retina and the optic nerve head; using the slit lamp, no anterior segment abnormalities were observed.

Electrophysiologic Function of the Retina and the Optic Nerve in *ALI030* Mutants

Due to poor responses in the head-tracking reflex observed in mutants by using the virtual drum, we used ERG and VEPs to investigate the functional integrity of the retinal neural circuitry and the electrical transmission in the visual pathway in vivo, respectively. We measured flash ERGs of these animals from dark- and light-adapted retinas to obtain rod- and cone-driven responses. The scotopic ERGs of the hetero- and homozygous mutants were similar to those of the wild types at different flash intensities (Fig. 2a). However, the a- and b-wave amplitudes appeared to be slightly smaller in homozygous mutants than in the wild types (**$P < 0.05$, ***$P < 0.01$; Fig. 2b). The photopic ERGs of the homozygous and heterozygous mutants were similar to those of the wild types at different flash intensities (Fig. 2c), except at the highest flash strength, where the a-wave amplitude was significantly reduced in both *ALI030* mutant groups compared to the wild types. The b-wave amplitude was significantly reduced in the homozygous mutants compared with the heterozygous mutants and wild types (Fig. 2d).

We also measured rod- and cone-driven flash VEPs in these animals. In the wild-type group, the scotopic VEP signals at low flash strengths initially showed one negative trough (N1) followed by one positive peak (P2). At higher flash strengths, a second positive peak (P1) became prominent and the signal amplitude increased (Fig. 2e). The scotopic VEP patterns of the hetero- and homozygous *ALI030* mutants were similar to those of wild-type mice at different flash strengths (Fig. 2e). We did not find any significant differences in the timing or amplitude of the analyzed signal parameters of the scotopic VEP between the wild types and mutants. Similar to the scotopic VEP, the photopic VEPs of the hetero- and homozygous *ALI030* mutants were comparable to the wild types, but the homozygous mutants showed slightly reduced amplitudes of N1

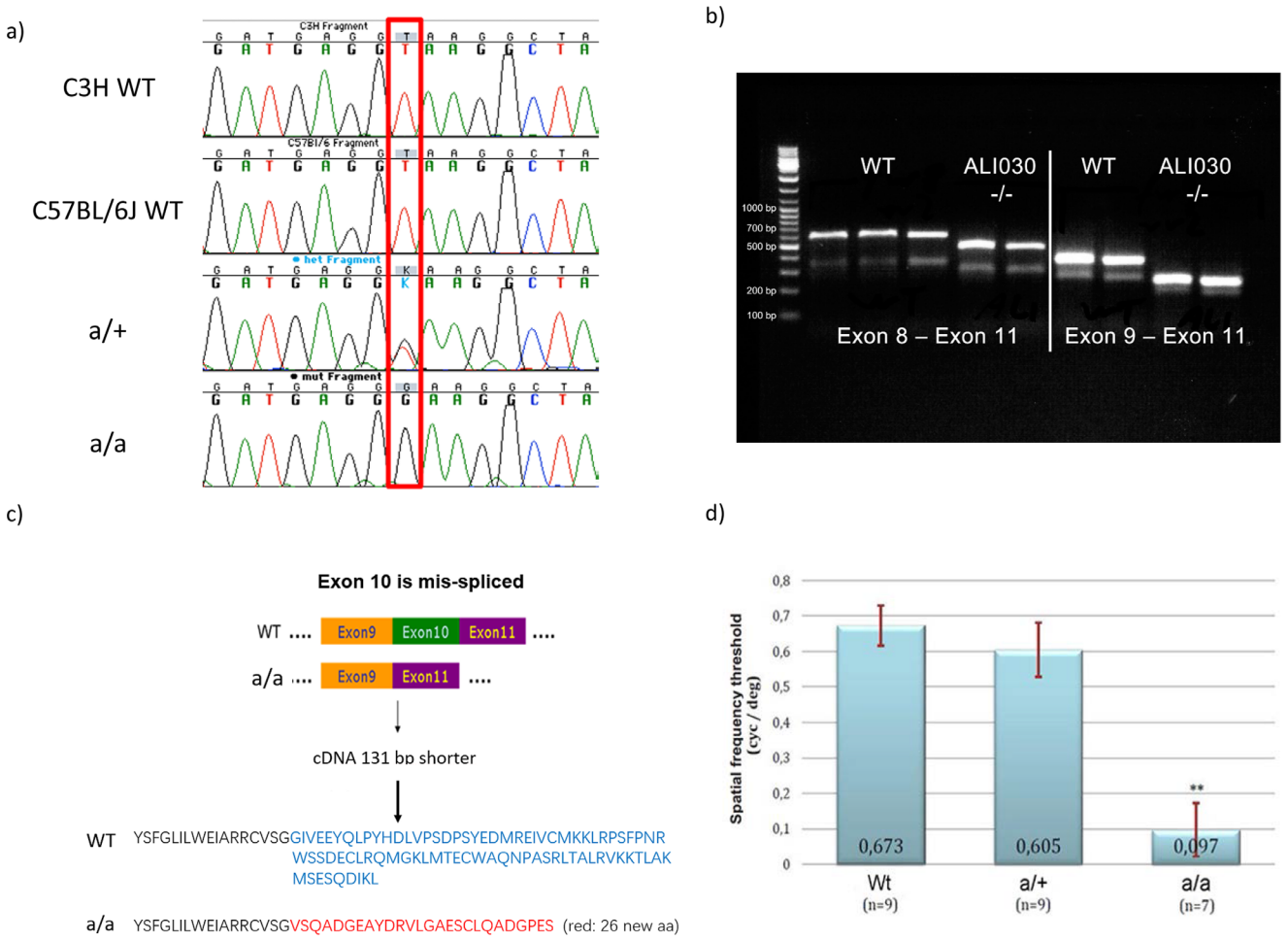

Figure 1. Genetics of the *ALI030* mutant mouse. (**a**) Genomic DNA sequence analysis of *Bmpr1b* of wild-type C3H and C57BL/6J mice as well as of heterozygous and homozygous *ALI030* mice. The site of the mutation is indicated by a *red box*; there is no difference between C3H and C57BL/6; homozygous mutants show the G instead of T; heterozygotes show both bases. (**b**) PCR products of cDNA spanning exon 8 to exon 11 (left) or exon 9 to exon 11 (right) are shorter in the homozygous mutants as compared with wild types. (**c**) Schematic drawing of the missplicing of exon 10 in the *ALI030* mutants, which results in 26 new amino acids with a premature stop codon. (**d**) Optokinetic drum test showed significantly reduced visual acuity in homozygous *ALI030* mutants compared to wild-type and heterozygous mice, all on C57BL/6J background (**$P < 0.001$; *bars*, standard deviation; *n*, number of mice at the age of 10 weeks).

over all flash intensities that were not significantly different from those of wild types (Fig. 2f). However, further analysis revealed that the P1 amplitude in the homozygous mutants was significantly reduced (by approximately 40%) compared to the wild types (**$P < 0.05$) (Fig. 2g), but no difference was found between heterozygous mutants and wild types. Both electrophysiologic methods demonstrated that under photopic conditions, the transmission of visual stimuli was impaired, explaining—at least in part—the loss of vision in the homozygous mutants as indicated by the missing head-tracking reflex.

The Phenotypes of the Optic Nerve Head and the Ventral Retina in *ALI030* Mutants

To analyze these severe ocular defects in detail, we investigated the optic nerve head (ONH) and retina by performing in vivo imaging (SD-OCT) and histology in *ALI030* mutants on the C57BL/6J background. SD-OCT revealed an optic disc coloboma indicated by an enlarged and very thin optic disc and a thicker inner plexiform layer in the ventral retina of the mutants ($n = 12$ eyes, six mice) compared to the wild types ($n = 10$ eyes, five mice) (Figs. 3a, A–D). OCT scans showed distinct retinal layers in the wild types (Figs. 3a, E). In the mutants, however, the distinct layers in most ventral retina disappeared, forming a zone extending from the retinal ganglion cell layer to the outer plexiform layer (Figs. 3a, F); some retinal areas showed a small zone (Figs. 3a, F, arrowhead), which was similar to the rosette-like structures found in the histologic study. Additionally, a long retinal glial scar-like structure was found in the ventral retina (Figs. 3a, G). Histology demonstrated retinal delamination and retinal rosette-like structures in the mutant ventral retina at different postnatal periods; moreover, at 5 months, the photoreceptor layer was severely disrupted in the mutants compared to the wild types (Figs. 3b, A–F, black circles). Additionally, a number of cells were aggregated in the inner plexiform layer (Figs. 3b, D and F, black arrows). The inner limiting membrane and the retinal ganglion cell layer in the ventral retina showed severe alterations with proliferating and migrating cells (Figs. 3b, A–F, black arrows). In addition,

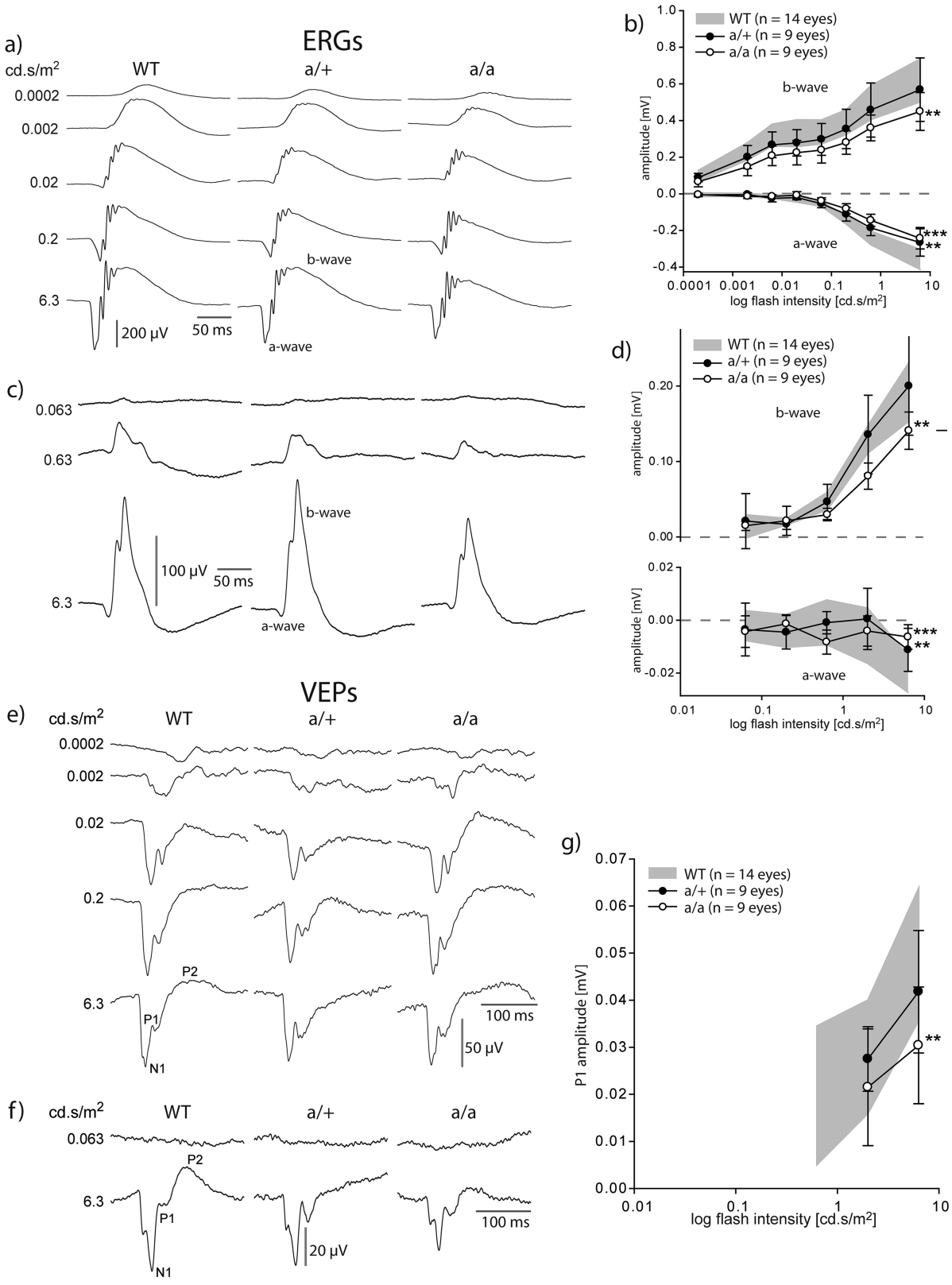

Figure 2. ERG and VEPs of *ALI030* mutant mice. (**a**, **b**) Scotopic flash ERGs of hetero- and homozygous *ALI030* mice are very similar to those of wild-type (WT) mice, although a small reduction of the amplitude can be observed in the mutant ERGs (**a**). The a- and b-wave amplitudes of the homozygous *ALI030* mutants are consistently smaller than those of the wild types and the heterozygous mutants at the highest flash strength (**b**) (**$P < 0.05$, ***$P < 0.01$). (**c**, **d**) Photopic flash ERGs of hetero- and homozygous *ALI030* mice are similar to those of WT mice, although a reduction of the b-wave amplitude is obvious in the homozygous mutants (**c**). The a- and b-wave amplitudes of the homozygous *ALI030* mutants are significantly smaller than those of the wild types and the heterozygous mutants at the highest flash strength (**d**) (**$P < 0.05$, ***$P < 0.01$). (**e**, **f**) Scotopic (**e**) and photopic (**f**) VEPs of hetero- and homozygous *ALI030* mutants are similar to

Investigative Ophthalmology & Visual Science

those of WT mice. Analysis of signal amplitudes and timing shows a general tendency of slightly reduced amplitudes of only N1 over all flash intensities that was not statistically significant. (**g**) Averaged amplitude (± SD) of the photopic P1 component as a function of flash strength for wild-type and *ALI030* heterozygous and homozygous mice. At the highest flash strength, homozygous *ALI030* mutants show a significantly reduced P1 amplitude compared to the wild types (**$P < 0.05$).

an enlarged optic disc coloboma was found in the mutants from early postnatal periods to adulthood (Figs. 3b, G–L, black arrow).

Then we analyzed the dysplasia of the retina in greater detail using different antibodies against specific retinal cell markers at P21. PDE6B is a marker for rod photoreceptors.[31,32] PDE6B immunostaining demonstrated a disruption and delamination of the photoreceptor layers in the mutant ventral retina compared to the wild types (Figs. 3c, A and E). Protein kinase Cα (gene symbol: *Prkca*) predominantly labels rod bipolar cells in the retina.[33] The lamination of retinal rod bipolar cells was disrupted in the ventral retinal gliotic region, and some ectopic bipolar cells were found in the outer nuclear layer of the mutants (Figs. 3c, B and F). OTX2 can control the fate of photoreceptors and the specification of the cells of the retinal pigment epithelium (RPE), and it is expressed in the inner nuclear layer and in the RPE.[34] Immunostaining against OTX2 showed that the inner nuclear layer was disrupted and split into two layers; the RPE was also disrupted, and fewer RPE cells were present in the ventral gliotic retina in *ALI030* mutants compared with wild-type controls (Figs. 3c, C and G).

Calretinin is considered a marker for the amacrine and ganglion cells of the retina.[35] In the wild types, calretinin is expressed in the retinal ganglion cells, amacrine cells, and inner plexiform layer, whereas in mutants, missing retinal ganglion cells are found in the inner plexiform layer and the retinal ganglion cell layer is thinner or missing in the gliotic retina (Fig. 3c, D–H). The amacrine cells are located in the inner nuclear layer in the wild types (Figs. 3c, D), whereas in mutants, the inner nuclear layer is totally disrupted in the ventral gliotic retina. Interestingly, there were some mislocalized amacrine cells in the inner plexiform layer (Figs. 3c, H). These results demonstrate that retinal dysplasia occurs in the ventral gliotic retina of the mutants.

In addition, retinal blood vessel abnormalities were observed in the mutants (Figs. 3a, A-B; Figs. 3d, A-C). In the ONH of the wild types, central retinal vessels were arranged regularly and retinal branch arterioles/veins originated from the central retinal artery/vein (Figs. 3d, A, B). However, in mutants, dilatation and distortion of retinal arterioles and venules was found, and some branch arterioles/veins did not arise directly from the central retinal artery/vein (Figs. 3d, C-E). The remnants of the hyaloid vessels were located at the peripheral part of the ONH in the mutants, whereas in the wild-type controls the vessels were located in the central part (Figs. 3a, A and B, white arrow; Figs. 3b, G–L, red arrowhead; Figs. 3d, A, C). The basement membrane of retinal arterioles was thickened in the mutants due to the replication of the lamina densa, one of the two components of the blood vessel basement membrane (Fig. 3e).

Activated Glial Cells in the ONH and in the Ventral Retina and Maldevelopment of the Optic Nerve in *ALI030* Mutants

Due to the findings in the retina by OCT and histology, we tested whether reactive gliosis is present in mutants. Glial fibrillary acidic protein (GFAP) is a reliable early marker of reactive gliosis in glial cells, and the expression of GFAP is upregulated during reactive gliosis.[36] Indeed, in the wild types at E17.5, GFAP is strongly expressed in the optic nerve (Figs. 4a, A and B) but weakly expressed in the nerve fiber layer and inner plexiform layer (Figs. 4a, E and F), whereas in mutants, GFAP is strongly expressed in different retinal layers in the ventral retina of the mutants (Figs. 4a, G and H). In the optic nerve, interestingly, GFAP is ectopically expressed around the retina in mutants (Figs. 4a, C and D), but not in wild types (Figs. 4a, A and B), suggesting that glial cells are also activated in the ONH during development and that ventral retinal gliosis is present at birth in the *ALI030* mutants. In addition, retinal folds were also formed in the ventral retina (Figs. 4a, G and H, arrowhead) and around the optic nerve (Fig. 4, D, arrowhead).

Furthermore, immunostaining against GFAP on flat-mounted retinas showed that activated glial cells were found in both the ONH and the ventral retina of the mutants (Figs. 4b, A–J) and formed a glial scar in the ventral retina, which was connected to the ONH (Figs. 4b, F and G). Immunostaining against GFAP on retinal sections also showed higher and more robust expression of GFAP in the ONH and in the ventral retina compared to wild-type controls (Figs. 4c, A–H). At different stages from P5 to adulthood, GFAP-positive cells were only found in the nerve fiber layer and retinal ganglion cell layer in the wild-type retina (Figs. 4c, A–D). However, in the mutants, GFAP was expressed in the inner and outer plexiform layer from P5 to adulthood (Figs. 4c, E–H). In the early postnatal period, activated glial cells were mainly located in the inner and outer plexiform layers, and retinal rosettes were absent, whereas in older animals (P21 and at 3 months), the range of retinal gliosis was more broad and extended to the inner nuclear layer and outer plexiform layer as well as to the inner plexiform layer (Figs. 4c, A–H). These results confirmed that the gliosis occurs in the ONH and in the ventral retina of the mutants.

Consistent with the activated astrocytes in the ventral retina of the mutants (Figs. 4d, A and B), transmission electron microscopy of the retina showed that astrocytes in the ventral gliotic retina were hypertrophic (Figs. 4d, C–F).

Activated Astrocytes Express SOX2 and PAX2 but Not PAX6 in Ventral Retinal Gliosis and Are Proliferative in *ALI030* Mutants

We analyzed the properties of these activated astrocytes in the gliotic ventral retina. Three different progenitor cell markers, SOX2, PAX2, and PAX6, were investigated. SOX2 (SRY [sex determining region Y]–box 2) is a transcription factor that is essential for stem cell pluripotency.[37] PAX2 (encoded by the paired box gene 2) is a transcription factor that can control the fate decision of neurons and glia.[38] *PAX6* (encoded by the paired box gene 6) is expressed in retinal progenitor cells and is essential for neuronal fate differentiation and determination in the retina[39] as well as neuro-

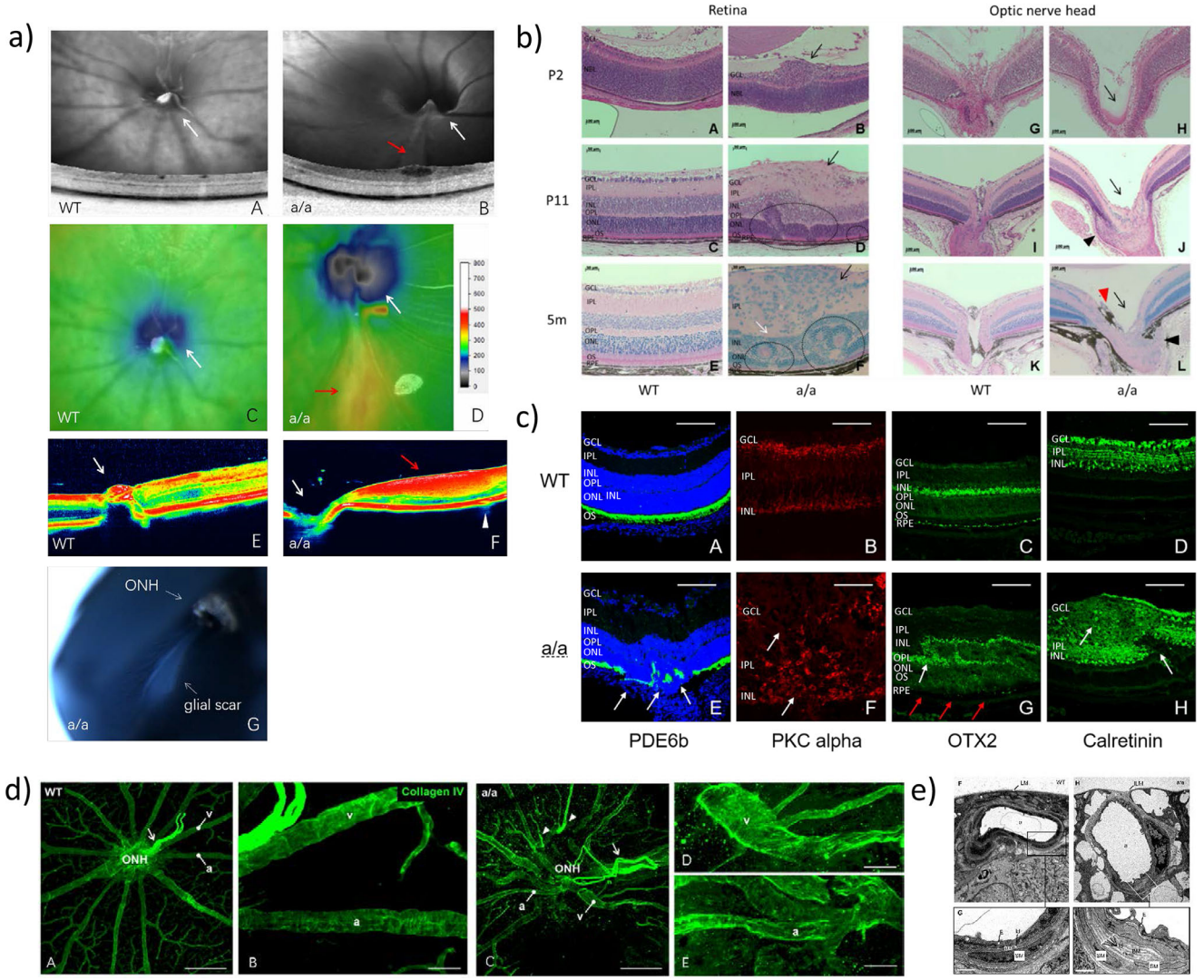

Figure 3. Retinal pathologies in *ALI030* mutants at 3 months. (**a**) SD-OCT showed excavation of the optic nerve head and a remarkable reduction in the central thickness in *ALI030* mutants (**A–F**, a/a, *white arrow*). The ventral retinal change is connected to the optic nerve head (**B**, **D**, *red arrow*). The changes manifest as an increasingly thick *red* layer on OCT scans of the ventral retina and affect multiple layers (**E**, **F**, a/a, *red arrow*). There are several defective regions similar to rosette structures found in the photoreceptor layer (**F**, *white arrowheads*). A long retinal glial scar-like structure was found in the ventral retina in the mutants (**G**, *white arrow*). The *color bar* in D represents the thickness of the retina or optic nerve head. *Upper color*, thicker; *lower color*, thinner. (**b**) At P2, there is local cell aggregation in the retinal ganglion cell layer in the mutants (**B**, *arrow*). At P11, the inner plexiform layer is thicker than in the wild type, and retinal layering is disrupted in the mutants. The retinal ganglion cell layer (GCL) is broken and the retinal cells grow out through the broken retinal GCL (**D**, *arrow*), in contrast to cells from the wild types (**C**, GCL). Moreover, retinal rosettes are found (**D**, *broken circles*). At the adult stage (5 months), the cell number in the inner plexiform layer is increased compared with early ages (**F**, *black arrow*), and the organization of the inner and outer nuclear layer and photoreceptor layer is severely altered (**F**) compared with those of the wild types (**E**). Some cells in the inner plexiform layer appear to be from the inner nuclear layer in the mutants (**F**, *white arrow*). Retinal rosettes are abundant in the outer retina of the mutants (**F**, *broken circles*). Excavation of the optic nerve head is found in the mutants at P2 (**H**, *arrow*), P11 (**J**, *arrow*), and adulthood (5 months) (**L**, *arrow*) but not in the wild types (**G**, **I**, **K**). There are more cells in the tip of the optic nerve head at P11 (**J**, *arrowhead*) and at adulthood (**L**, *black arrowhead*) in the mutants. Remnants of the hyaloid artery are found in the rim of the optic nerve head (**L**, *red arrowhead*) in the mutants. GCL, ganglion cell layer; IPL, inner plexiform layer; INL, inner nuclear layer; NBL, neuroblast layer; NFL, nerve fiber layer; ONL, outer nuclear layer; OPL, outer plexiform layer; OS, outer segment of photoreceptors; RPE, retinal pigment epithelium. *Scale bar*: **A**, **B**, **G–L**, 100 µm; **C–F**, 50 µm. (**c**) At P21, regular retinal lamination and different types of retinal cells are found in the wild types. PDE6B is expressed in the photoreceptor layer (**A**); protein kinase Cα (PKC-α) is expressed in the bipolar cells (**B**); OTX2 is expressed in the inner nuclear layer and in the RPE (**C**); calretinin is expressed in the immature neurons of the retinal ganglion cell layer, inner plexiform layer, and inner nuclear layer (**D**). However, delamination, thinner photoreceptors, and photoreceptor rosettes are found in the mutants (**E**). The synaptic connections and axons of the bipolar cells are destroyed in the mutants (**F**, *arrow*). The inner nuclear layer splits into two layers (**G**, *white arrow*) and a remarkably decreased number of RPE cells are found (**G**, *red arrow*). The retinal ganglion cell layer is disrupted, some ectopic calretinin-positive neurons are found in the inner plexiform layer (**H**, *arrow*, *above*), and the inner nuclear layer is destroyed in mutants (**H**, *arrow*, *below*). *Scale bar*: 50 µm (**A**, **C–E**, **G**, **H**); 20 µm (**B**, **F**). (**d**) Whole-mount immunofluorescence against collagen IV shows several retinal arterioles originating independently from the central retinal artery in the central excavation of the ONH (**A**, *arrowheads*). (**e**) Electron microscopy shows venular dilatation and arteriole disruption as well as basement membrane thickening due to replication of the lamina densa in the mutant mice. ONH, optic nerve head; v, venule; a, arteriole; Id, lamina densa; ILM, inner limiting membrane; E, endothelial cell; SM, smooth muscle cell; BM, basement membrane; GCL, ganglion cell layer. *Scale bars*: 0.4 µm (**G**, **I**).

Investigative Ophthalmology & Visual Science

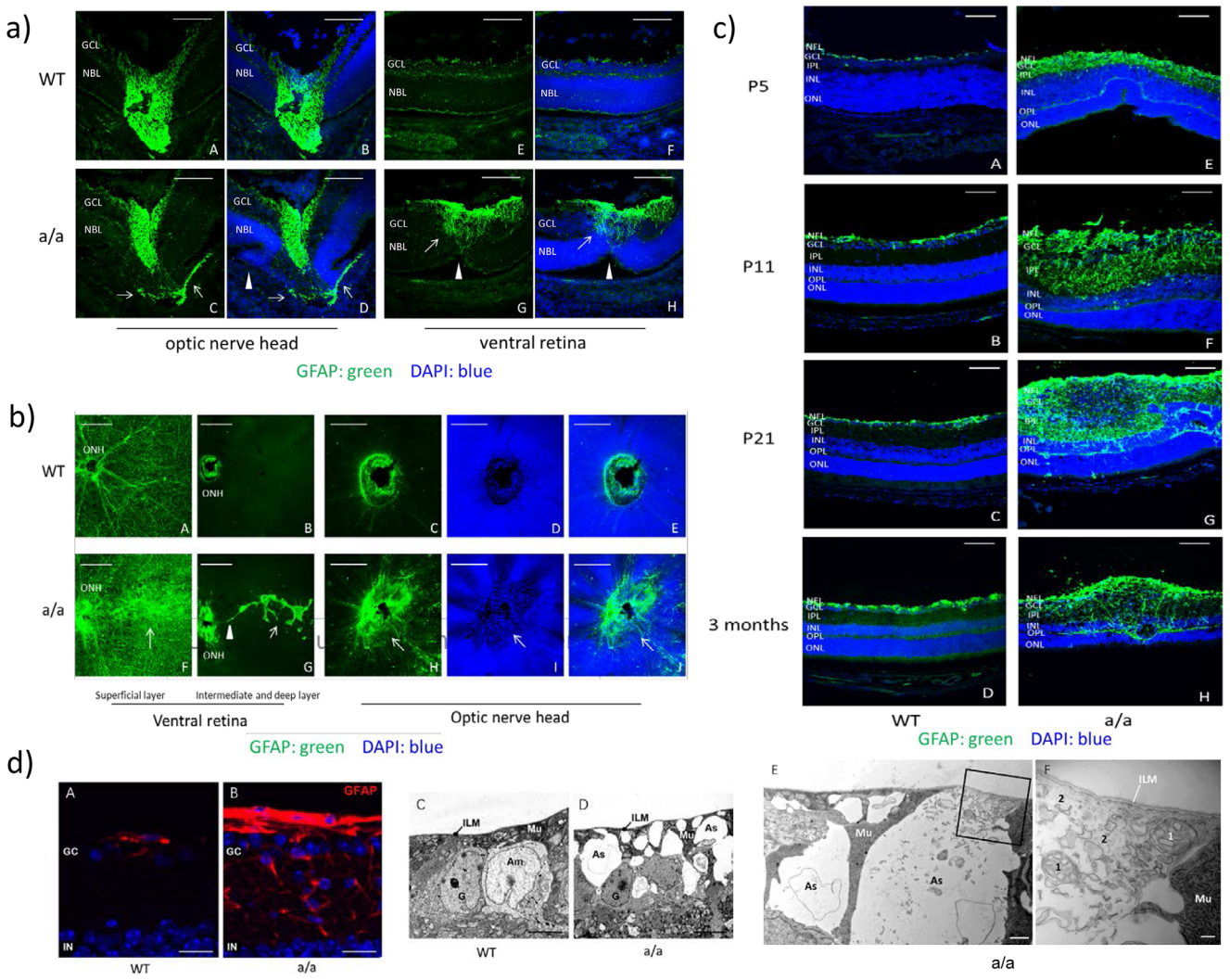

Figure 4. Gliosis in the ventral retina and optic nerve head in *ALI030* mutants. (**a**) (**A**) At E17.5, GFAP is strongly expressed in the optic nerve in the wild types (**A**, **B**), whereas in the mutants, besides in the optic nerve, GFAP is also ectopically expressed around the retina (**C**, **D**, *arrows*). (**E**, **H**) GFAP is weakly expressed in the nerve fiber layer and inner plexiform layer of the wild-type retina at E17.5, whereas it is strongly ectopically expressed in the ventral retina in the mutants (**G**, **H**). *Scale bar*: 50 µm. (**b**) Immunostaining against GFAP on retinal flat-mount preparations showed that glial scarring occurs in the ventral mutant retina (**F**, **G**) compared with the wild types (**A**, **B**), and gliosis in the optic nerve head (ONH) was found (**H–J**, *arrow*) in mutants. The ventral glial scar is connected to the optic nerve head (**G**, *arrowhead*). *Scale bar*: **A**, **B**, **F**, **G**, 300 µm; **C–E**, **H–J**, 200 µm. (**c**) Ventral retinal gliosis in the *ALI030* mutants from P5 to 3 months. (**A–D**) In the wild types, GFAP is expressed in the retinal ganglion cell layer and nerve fiber layer. (**E–H**) Strong GFAP expression is found in distinct retinal layers, especially in the inner plexiform layer, where the number of activated glial cells is significantly increased. At P5, the expression of GFAP is significantly upregulated in the outer plexiform layer in the mutants (**E**), and later the retinal gliosis is broader and more intense in the outer plexiform layer in adults compared with the early periods. The retinal fold is formed at P5 (**E**) and later retinal rosettes are formed at P21 (**G**) and at 3 months (**H**). NFL, nerve fiber layer; GCL, ganglion cell layer; IPL, inner plexiform layer; INL, inner nuclear layer; OPL, outer plexiform layer; ONL, outer nuclear layer. *Scale bar*: 50 µm. (**d**) Overexpression of GFAP (**A**, **B**) and the presence of enlarged astrocytic prolongations between ganglion cells (**C**, **D**), characterized by a clear cytoplasm containing mitochondria and intermediate filaments (**E**, **F**) by electron microscopy, clearly suggest astrocytic hypertrophy in *ALI030* mutants. GC, ganglion cell layer; IN, inner nuclear layer; ILM, internal limiting membrane; G, ganglion cell; Am, amacrine cell; As, astrocyte; Mu, Müller cell. *Scale bars*: 16 µm (**A**), 4.5 µm (**B**), 0.45 µm (**C**).

genesis.[40] We found that in mutants, the main cell type of activated glial cells in the ventral retina were astrocytes, since most cells expressed GFAP but not glutamate synthase, a marker for retinal Müller cells (Figs. 5a, A–H). Interestingly, on the vitreal side of the retinal gliotic region, OCT showed a thick epiretinal membrane-like structure (Figs. 3a, D, red arrow; F, red arrow), where GFAP was highly and densely expressed (Figs. 5F). Here, in the inner plexiform layer and inner nuclear layer, GFAP was mainly expressed in the cytoplasm and SOX2 was expressed in the nucleus of the same cells (Fig. 5b), suggesting that the activated astrocytes also express SOX2.

PAX2 was expressed in the retinal ganglion cell layer, and some PAX2-positive cells also expressed SOX2 in the wild types (Figs. 5c, A–D), but PAX2 was highly expressed in almost all cells in the ventral retinal gliosis region of the mutants (Figs. 5c, E). It was localized in the nucleus and was also coexpressed with SOX2 in the ventral gliotic region

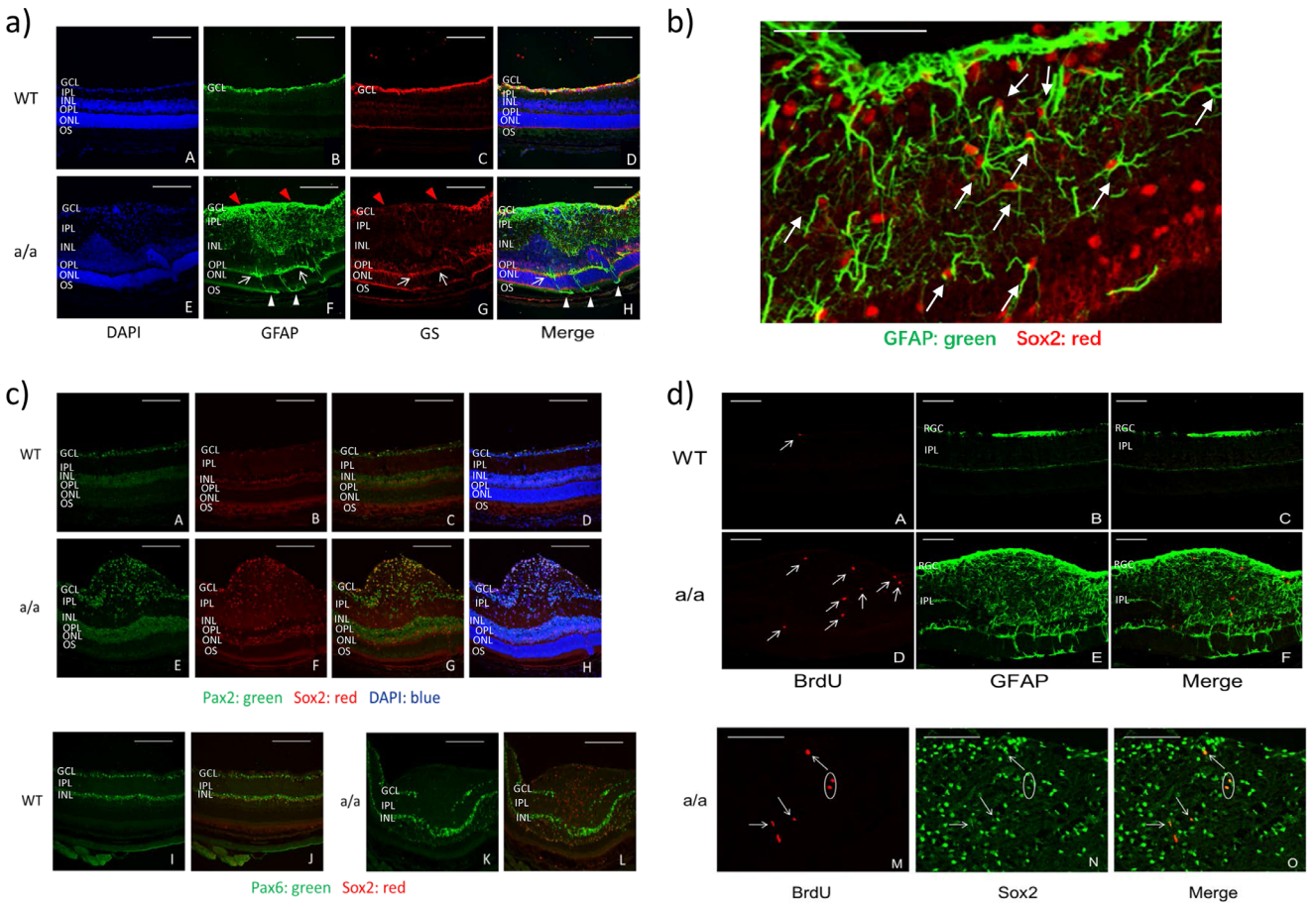

Figure 5. Activated astrocytes expressing progenitor cell markers and proliferative retinal gliosis in *ALI030* mutants at P21. (**a**) (**A–D**) Glutamate synthase (GS) is normally expressed in the nerve fiber and retinal ganglion cell layer, and it coexpresses with GFAP. (**E–H**) In the mutants, a few activated glial cells coexpress GS. Most GFAP-positive cells do not express GS, suggesting that the main glial cells are activated astrocytes. *Scale bar*: 50 µm. (**b**) In the gliotic retina, almost all activated astrocytes express SOX2. SOX2 overlaps with GFAP in the vitreal side of the retina (**C**, *yellow*), whereas in the other retinal layers, GFAP is expressed in the cytoplasm and SOX2 is expressed in the nuclei of the same cells (**A–F**). *Scale bar*: 100 µm. (**c**) (**A–D**) In wild-type retina, a few PAX2-positive cells express SOX2 in the retinal ganglion cell layer. (**E–H**) In the mutants, there are a number of activated astrocytes expressing PAX2 in the distinct retinal layers. (**I**, **J**) PAX6-positive cells normally coexpress SOX2 in the retinal ganglion cell layer and inner nuclear layer, whereas most activated astrocytes do not express PAX6 in the mutants (**K**, **L**). *Scale bar*: 50 µm. (**d**) In wild-type retina, there are very few BrdU-positive cells (**A–C**), but there are a remarkably increased number of BrdU-positive cells in the ventral retinal gliotic region (**D–F**). Most of these BrdU-positive cells coexpress SOX2 (**M–O**). *Scale bar*: 100 µm.

(Figs. 5c, E–H). PAX6 was expressed in the retinal ganglion cell layer and inner nuclear layer in wild-type retina (Figs. 5c, I and J), whereas in mutants, PAX6 was almost absent in the ventral gliotic region (Figs. 5c, K and L). These data suggest that these ventral activated glial cells may have properties of retinal progenitor cells.

To further investigate whether these activated glial cells expressing progenitor cell markers in the ventral retina were proliferative, BrdU was injected intraperitoneally to label proliferating cells at P21. As shown by BrdU-labeled cells, we found proliferating glial cells in the inner plexiform layer of the ventral gliotic retina of the mutants at P21 (Figs. 5d, D), whereas very few BrdU-positive cells were found in the wild-type retina (Figs. 5d, A). Interestingly, most of these BrdU-positive cells also coexpressed SOX2 (Figs. 5d, M–O). Therefore, proliferative retinal gliosis occurs in the mutants. This proliferative ability could be due to the progenitor property of the activated astrocytes.

Altered Eye Development, Loss of Ventral Retinal Ganglion Cells, Axon Misguidance, and Downregulation of pSMAD1/5/8 in *ALI030* Mutants

To understand these histologic and electrophysiologic findings, we investigated the embryonic development of the eyes of *ALI030* mutants. From knockout mutants, we know that *Bmpr1b* is expressed in the ventral retina and is required for correct targeting of ventral ganglion cell axons to the ONH. Moreover, many axons arising from the ventrally located ganglion cells fail to enter the ONH and instead make abrupt turns in this region.[14] PAX2 is one of the major players in ONH development and optic fissure closure in the ventral retina.[41,42] The expression pattern of PAX2 was dynamically changed in mutants during embryonic retinal development compared to wild types (Figs. 6a, A–H). At E10.5, PAX2 was expressed in the ventral retina and the optic stalk in the

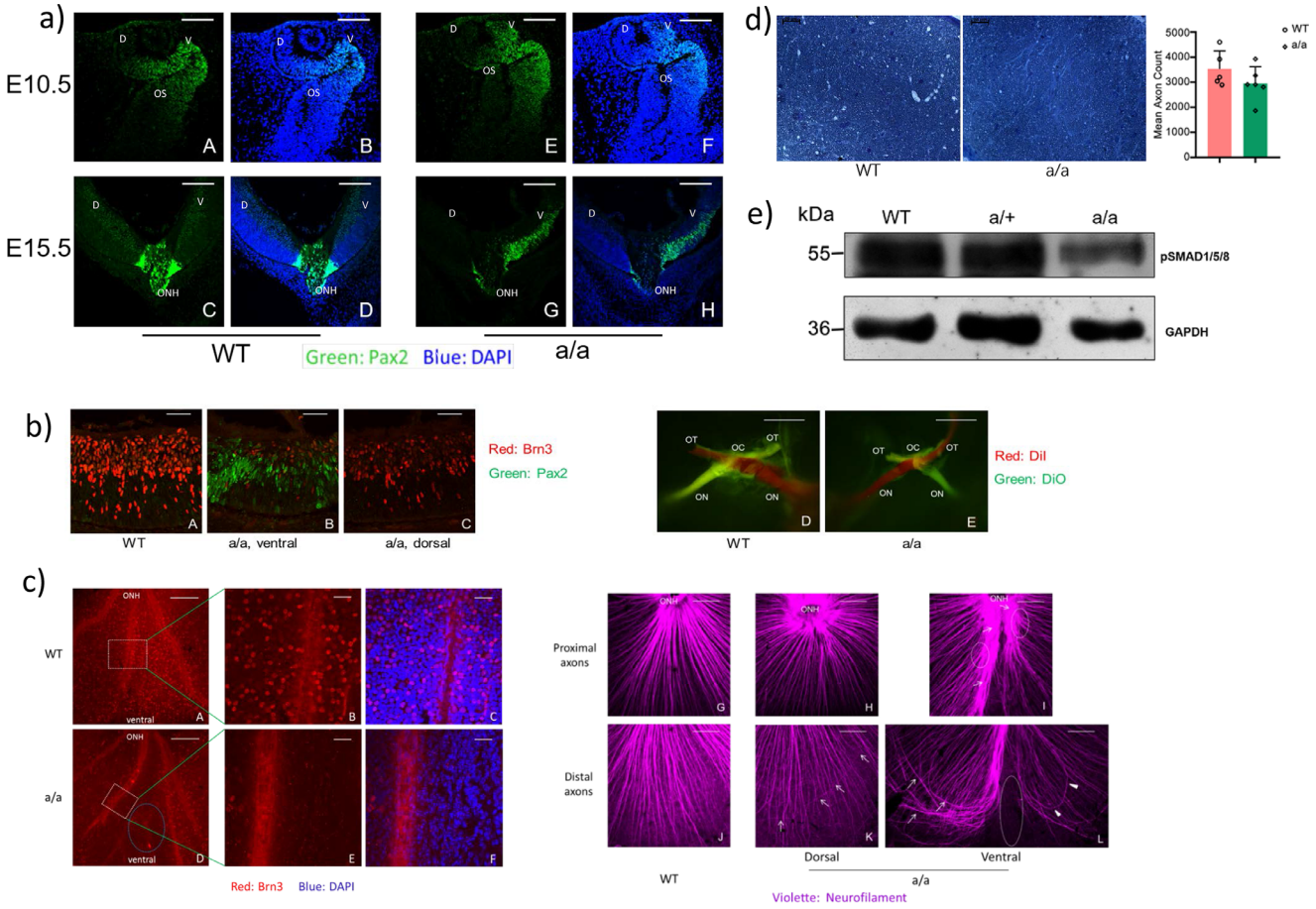

Figure 6. Ectopic PAX2 expression, decreased neurogenesis of retinal ganglion cells, and downregulation of pSMAD1/5/8 in *ALI030* mutants. (**a**) PAX2 expression at E10.5 in the ventral retina and in the optic stalk in the wild types (**A**, **B**) and homozygous *ALI030* mutants (**G**, **H**). No difference was found between the wild types and mutants. At later stage, E15.5, PAX2 is expressed in the optic nerve–retina junction and in the optic nerve head in the wild types. However, at E15.5, PAX2 expression is ectopically upregulated in the ventral retina and decreased in the dorsal junction between optic nerve and retina in mutants (**I**, **J**). D, dorsal retina; ON, optic nerve; OS, optic stalk; V, ventral retina. *Scale bar*: 50 µm. (**b**) In the wild-type retina, there are a number of retinal ganglion cells (BRN3, *red*) but very few expressing PAX2 (*green*; **A**), whereas in the mutant retina, many cells express PAX2 in the ventral retina (**B**). Retinal ganglion cells production is greatly decreased in the ventral retina (**B**) but only slightly decreased in the dorsal retina (**C**) at E15.5. (**D**, **E**) Anterograde tracing demonstrated normal crossing and fasciculation of the optic nerve and optic chiasm in the mutants, but the optic nerve tends to be thinner in the homozygous mutants than in the wild-type controls, which is due to the decreased number of retinal ganglion cells at E15.5. OC, optic chiasm; ON, optic nerve; OT, optic tract. *Scale bar*: **A–C**, 20 µm; **D**, **E**, 100 µm. (**c**) Immunostaining against BRN3 on retinal flat-mount preparations showed that retinal ganglion cells are almost absent in the ventral gliosis retina in the mutants (**D–F**) compared to the wild types (**A–C**) at 3 months. The number of retinal nerve fibers is also decreased in the ventral retina, especially in the distal area, in the mutants (**L**, *broken circle*); the proximal retina exhibits two bundles of axons (**I**, *arrow*), and nearly all the retinal axons from the periphery directly enter one of the two bundles instead of the optic nerve head (**I**, *broken circle*). Mislocalized axons are found in the distal ventral (**L**, *arrow* and *arrowhead*) and dorsal retina (**K**, *arrow*) in the mutants. *Scale bar*: **A**, **D**, 300 µm; **B**, **C**, **E**, **F**, 50 µm; **G–L**: 300 µm. (**d**) The number of optic nerve axons in the mutants ($n = 6$) tends to be less than that in the wild types ($n = 5$) at 8 weeks, but no statistical significance is found ($P > 0.05$). (**e**) Western blot analysis showed that at 3 weeks in mutant retina, the expression level of pSMAD1/5/8 is lower than that in the wild types and heterozygous mutants, but no obvious difference was found between the wild types and heterozygous mutants.

wild types, and the expression of PAX2 was not affected in mutants compared to the wild types (Figs. 6a, A and B, E and F). At E15.5, PAX2 was expressed in the ventral retina and the expression in the ONH, including the dorsal junction, was reduced in mutants, whereas it was only expressed in the retina–optic nerve junction in the wild types (Figs. 6a, C and D, G and H).

Consistent with the PAX2 results, immunostaining against BRN3 (also known as POU4F1), a marker for retinal ganglion cells,[43,44] showed that the neurogenesis of retinal ganglion cells was decreased (Figs. 6b, A–C) in the mutants at E15.5. Similarly, after 3 months, retinal ganglion cells in the mutants were almost absent in the ventral gliosis retina compared with the wild types (Figs. 6c, A–F; Supplementary Fig. S3). In this region, there were two bundles of axons on both sides near the central ventral retina, and almost none of the axons in the ventral retina entered the ONH but instead went into these two bundles (Figs. 6c, I). In addition, mislocalized axons were found in the peripheral ventral retina as well as in the dorsal retina in the mutants (Figs. 6c, K and L). Furthermore, anterograde tracing showed that there were no obvious differences in the crossing and fasciculation of the optic nerve and optic chiasm between the wild types and the homozygous mutants (Figs. 6c, D and E). However,

the optic nerve tended to be thinner in the mutants ($n = 7$ embryos) compared to the wild-type controls at E15.5 ($n = 5$ embryos), but no statistical significance was found ($P = 0.0524$) (Figs. 6c, D and E). Similarly, toluidine blue staining showed that fewer optic nerve axons were found in the mutants ($n = 6$) than wild types ($n = 5$), but there is no statistical significance (Fig. 6d).

To investigate the impact of the *Bmpr1b* mutation on BMP signaling in vivo, we tested the expression level of pSMAD1/5/8 in the retina by using Western blot at 3 weeks. We showed that in the mutant retina, the expression level of pSMAD1/5/8 was slightly lower in the homozygous mutants than in the wild types and heterozygous mutants, but no obvious difference was found between the wild types and the heterozygous mutants (Fig. 6e).

Discussion

Reactive gliosis occurs in various grades; however, massive retinal gliosis is considered to result frequently in a glial scar.[45] Here, we characterized a new mouse model of optic disc coloboma and ventral retina gliosis, which is caused by an ENU-induced splice site mutation in *Bmpr1b*. This mutation in intron 10 of *Bmpr1b* results in the skipping of exon 10, leading to a translational frame shift and a premature stop codon; it is predicted that the conserved cytoplasmic serine/threonine kinase domain is lost in the mutants. This point mutation leads to a more severe and newer phenotype compared with the corresponding knockout mutant.[14]

In humans, optic disc coloboma is characterized by a demarcated bowl-shaped excavation in the optic disc caused by incomplete closure of the optic fissure during embryonic development.[46] Visual deficits correlate with the severity of the morphologic anomaly. Optic disc coloboma is often associated with other ocular anomalies or even syndromic disorders. There are several genetic conditions known to lead to optic disc coloboma, such as mutations in *PAX2*, *PAX6*, *SHH*, or *CHX10*.[47] However, the detailed pathogenesis of this disease is still poorly understood even if there have been several animal models established. Therefore, we focused on a detailed analysis of the formation of optic disc coloboma and retinal gliosis in the new *Bmpr1b* mutant.

The first most striking effect of this mutation is the significant decrease of the head-tracking reflex as observed in an optokinetic drum. However, ERG measurements showed significant reductions of the scotopic and photopic a- and b-wave amplitudes at the higher flash intensities. Also, VEP measurements showed a general tendency toward slightly smaller amplitudes of N1 (scotopic VEPs) and of N1 and P1 (photopic VEPs) over all flash intensities, with significant reductions of N1P1 amplitudes at the higher flash intensities. Since the gliosis is restricted to the ventral retina, the visual field is expected to be smaller in the mutants, which might lead to a relatively larger effect on the perception of moving stripes in the optokinetic drum versus stationary flashing light as is used in the ERG and VEP. Similarly, patients with coloboma involving optic disc also showed slight ERG changes but more obvious VEP changes. In addition, increased eye axial length was found in mutants, which could be due to optic nerve coloboma. This could contribute to a larger refractive error, leading to decreased visual acuity. Another striking finding is the detection of ONH coloboma in the mutants. The ONH coloboma was found in the very early postnatal period such as P5, suggesting that this abnormality is arising from maldevelopment of the ONH. The glial cells in the ONH were activated, the processes of the glial cells in the ONH showed disorganized arrangements, and some axons in the optic nerve were absent, indicating a degenerative change in the optic nerve. However, these features do not explain the occurrence of a coloboma, which might be explained better by the decreased *PAX2* expression in our novel *Bmpr1b* splice-site mutants (see below for greater detail).

At the histologic level, we observed retinal delamination, rosettes, and altered retinal blood vessels in the mutants. These features have also been found in other eyes with coloboma.[48,49] Similar to human patients with fundus coloboma,[49] several retinal arterioles did not arise directly from the central retinal artery in the new *Bmpr1b*-mutant mice. Moreover, as in rats with optic disc coloboma,[48] dilatation and distortion of retinal arterioles and venules were common in the *Bmpr1b*-mutant mice. Missense mutations of the human *BMPR1B* gene produce idiopathic pulmonary arterial hypertension during childhood,[50] and blood vessel basement membrane thickening results from a common arterial lesion during this disease.[51] We also observed blood vessel basement membrane thickening in the retinal arterioles of the *Bmpr1b*-mutant mice. Altogether, BMPR1B (or BMP signaling in general) may also be involved in retinal blood vessel development.

In *Bmpr1b*-knockout mice, abnormal axon guidance was found in the ventral retina during embryonic eye development.[14] In agreement with previous findings, we observed that a number of retinal ganglion cell axons entered the axon bundles instead of the ONH in the ventral retina, and a few axons were also mislocalized in the dorsal retina in the mutants. Therefore, we further analyzed the morphology of the optic nerve and optic chiasm at E15.5, when the optic chiasm was already mature. We found that axon guidance within the optic nerve and the optic chiasm was not affected in the mutants. These results indicate that BMPR1B may play a role in axon guidance in the retina but not in the higher visual pathways.

Several studies have shown that mutations in the *PAX2/Pax2* gene are associated with or are even the cause of optic nerve coloboma in humans[52] and mice.[53,54] The number of axons is also reduced in mice with *Pax2* mutations.[55] Reduced expression of PAX2 may also lead to the reduced expression of the Fas-associated death domain (*Fadd*) gene, which causes an open optic fissure by a proliferation defect and concomitant activation of the necroptosis pathway.[56] In contrast to the symmetrical expression of PAX2 in the ONH region of the wild types at E15.5 and E17.5, we found that PAX2 was ectopically expressed in the ventral retina and asymmetrically expressed in the ONH of the mutants. Therefore, *Bmpr1b* mutation changes the expression pattern of PAX2 during embryonic development, which may lead to a delay of the closure of the optic fissure and, subsequently, to optic disc coloboma. We also found that the expression of pSMAD1/5/8 in the retina was reduced in the mutants compared to the wild types, indicating that BMP signaling is affected by the mutation. The relationship between BMP signaling and *PAX2* remains unclear. Since BMP7 interacts with sonic hedgehog (SHH) to regulate *Pax2* expression in astrocytes,[57] we hypothesize that BMP signaling might also regulate the expression of *Pax2* in the retina. Meanwhile, the number of retinal ganglion cells is reduced in the ventral retina where PAX2 is ectopically expressed during embryonic retinal development. Later, at postnatal periods, retinal ganglion cells were almost absent,

Investigative Ophthalmology & Visual Science

suggesting that decreased neurogenesis of retinal ganglion cells is induced by overexpression of PAX2.

In our mutants, the altered PAX2 expression might also be one characteristic leading to gliosis of the ventral retina. Retinal gliosis is proliferative (as indicated by the GFAP and BrdU immunostaining) and hypertrophic and is associated with decreased neurogenesis in retinal ganglion cells. The activated astrocytes in the ventral gliotic retina are likely to be gliogenic precursors due to their proliferation and the expression of progenitor cell markers, such as SOX2. This particular phenotype was not described for the *Bmpr1b*-knockout mouse where bipolar cells are affected and neurogenesis remains unchanged.[14]

Previous studies have shown that migration of immature astrocytes from the optic nerve onto the inner surface of the retina is required for the generation of mature astrocytes.[58] In the *ALI030* mutants, we found ectopically activated glial cells across the different layers of the ventral retina, suggesting that these glial cells may occur after migration or originate from retinal progenitors. In-vivo BrdU labeling revealed that the activated glial cells proliferate in the postnatal eye and that these glial cells express PAX2 and SOX2 but not PAX6. PAX2 can inhibit the fate of neurons but promotes the differentiation of glial cells,[38] and PAX6 is known to be required for neuronal differentiation.[59] In addition, astrocytes can acquire the properties of stem cells and become multipotent cells during reactive gliosis induced by brain injury.[60]

In contrast to most other studies, in which reactive gliosis was induced by toxic chemicals or injury, our study demonstrated ventral retinal gliosis to be caused by a genetic defect. Similarly, the Bmp signaling pathway is shown to be necessary for oligodendrocyte maturation in the brain.[61] Following spinal cord injury, *Bmpr1b*-null mice developed hyperactive reactive astrocytes and had attenuated glial scars.[62] In conditional double-knockout mutants of *Bmpr1a* and *Bmpr1b* in the neural tube, fewer activated astrocytes were observed than in the wild types due to the defect in glial cell maturation.[63] Consistent with Lee et al.,[64] our mutant mice showed ventral retinal gliosis and an increased number of GFAP-positive astroglia in the ventral retina and ONH from early postnatal days to adulthood. These activated glial cells form a long aggregate with branches from the ONH to the ventral retina, which then extend into different retinal layers. In addition, it has been reported that BMP7 regulates reactive gliosis in retinal astrocytes and Müller cells and that BMP7 treatment of glial cells induces reactive gliosis in mice,[16] but microglial activation is required for this gliosis process.[65] Compared with both studies, ventral retinal gliosis is dominated by activated astrocytes and is a developmental process in our study, which is quite different. Our results indicate that *Bmpr1b* signaling may play a role in regulating the differentiation of gliogenic precursor populations in the retina.

Thus, these findings suggest that the activated glial cells in the ventral retina probably have properties of precursor cells of gliogenic populations (PAX2) but not of neurogenic populations (PAX6). Here, the deficiency in *Bmpr1b* might result in more gliogenic precursor populations in the retina, which is also consistent with previous work[64] demonstrating that inhibition of BMPR1B expression in primary glioblastomas can expand the clonogenic stem cell population.

In addition, retinal dysplasia was associated with ventral retinal gliosis in the mutants. The ventral gliotic retina exhibited dysplasia conditions in mutants, including retinal delamination and retinal rosettes. The synapses of the bipolar cells were disrupted (Fig. 4c) and ectopic retinal ganglion cells were found in the inner plexiform layer. These retinal changes might be due to the abnormal retinal development and the gliosis.

In addition to eye phenotypes, systemic phenotyping of the mutant mice revealed decreased body weight, which is associated with decreased bone mineral content and fat mass, reduced blood lipids and proteins, and generally complex effects on energy assimilation. The increased locomotion (at least in males) might be one aspect of this complex situation, because it indicates a higher use of energy, which might in turn be responsible for the alterations in the energy supply. These findings are in contrast to previously reported data showing that a deletion of *Bmpr1b* causes no obvious other defects besides skeletal deficits.[66]

In summary, we characterized a mouse model of ONH coloboma and ventral retinal gliosis caused by a mutation in *Bmpr1b*. Our work showed that BMPR1B is necessary for the development of the optic nerve and ventral retina. Since these results also help to significantly advance the understanding of the intrinsic mechanisms of retinal gliosis, it opens new routes for the treatment of gliosis that eventually might prevent scar formation in the retina.

Acknowledgments

The authors thank Erika Bürkle, Tommy Fuchs, Sandra Hoffmann, Nicole Lindemann, Andreas Mayer, Veronica Melgarejo, Lorena Noya, Maria Kugler, Michael Schulz, and Monika Stadler for expert technical assistance; Heike Hohwieler was involved in this project during an internship.

Supported by National Genome Network Grants (www.ngfn.de; NGFN, NGFN plus; grant identifications: BMBF 01KW9923 and BMBF 01GS0850), EUMODIC (European Mouse Disease Clinic, http://www.mousephenotype.org/news/eumodic-paving-way-impc-0; grant identification: LSHG-2006-037188), and Infrafrontier (www.infranfrontier.eu; grant identification 01KX1012). This project was also supported by grant JCYJ20170413143051465 from the Research Foundation of Science and Technology Plan Project, Shenzhen, China, grant 2016A020216002 from the Research Foundation of Science and Technology Plan Project, Guangdong, China, and grant 81970790 from National Natural Science Foundation of China. XY received a fellowship from the China Scholarship Council (http://en.csc.edu.cn/). DR was supported by Foundation for Science and Technology (grant number SFRH/BPD/102573/2014), Ministry of Education and Science, Portugal. The funders had no role in study design, data collection and analysis, decision to publish, or preparation of the manuscript.

Disclosure: **X. Yan,** None; **J. Atorf,** None; **D. Ramos,** None; **F. Thiele,** None; **S. Weber,** None; **C. Dalke,** None; **M. Sun,** None; **O. Puk,** None; **D. Michel,** None; **H. Fuchs,** None; **M. Klaften,** None; **G.K.H. Przemeck,** None; **S. Sabrautzki,** None; **J. Favor,** None; **J. Ruberte,** None; **J. Kremers,** None; **M. Hrabe de Angelis,** None; **J. Graw,** None

References

1. Reis LM, Tyler RC, Schilter KF, et al. *BMP4* loss-of-function mutations in developmental eye disorders including SHORT syndrome. *Hum Genet*. 2011;130:495–504.
2. Furuta Y, Hogan BL. BMP4 is essential for lens induction in the mouse embryo. *Genes Dev*. 1998;12:3764–3775.

3. Sakuta H, Suzuki R, Takahashi H, et al. A BMP-4 antagonist expressed in a double-gradient pattern in the retina. *Science*. 2001;293:111–115.
4. Trousse F, Esteve P, Bovolenta P. Bmp4 mediates apoptotic cell death in the developing chick eye. *J Neurosci*. 2001;21:1292–1301.
5. French CR, Erickson T, French DV, Pilgrim DB, Waskiewicz AJ. Gdf6a is required for the initiation of dorsal-ventral retinal patterning and lens development. *Dev Biol*. 2009;333:37–47.
6. Bakrania P, Efthymiou M, Klein JC, et al. Mutations in BMP4 cause eye, brain, and digit developmental anomalies: overlap between the BMP4 and hedgehog signaling pathways. *Am J Hum Genet*. 2008; 82:304–319.
7. Dudley AT, Lyons KM, Robertson EJ. A requirement for bone morphogenetic protein-7 during development of the mammalian kidney and eye. *Genes Dev*. 1995;9:2795–2807.
8. Luo G, Hofmann C, Bronckers ALJ, et al. BMP-7 is an inducer of nephrogenesis and is also required for eye development and skeletal patterning. *Genes Dev*. 1995;9:2808–2820.
9. Wawersik S, Purcell P, Rauchman M, et al. BMP7 acts in murine lens placode development. *Dev Biol*. 1999;207:176–188.
10. Morcillo J, Martinez-Morales JR, Trousse F, Fermin Y, Sowden JC, Bovolenta P. Proper patterning of the optic fissure requires the sequential activity of BMP7 and SHH. *Development*. 2006;133:3179–3190.
11. Faber SC, Robinson ML, Makarenkova HP, Lang RA. Bmp signaling is required for development of primary lens fiber cells. *Development*. 2002;129:3727–3737.
12. Hocking JC, McFarlane S. Expression of Bmp ligands and receptors in the developing Xenopus retina. *Int J Dev Biol*. 2007;51:161–165.
13. Du Y, Xiao Q, Yip HK. Regulation of retinal progenitor cell differentiation by bone morphogenetic protein 4 is mediated by the smad/Id cascade. *Invest Ophthalmol Vis Sci*. 2010;51:3764–3773.
14. Liu J, Wilson S, Reh T. BMP receptor 1b is required for axon guidance and cell survival in the developing retina. *Dev Biol*. 2003;256:34–48.
15. Murali D, Yoshikawa S, Corrigan RR, et al. Distinct developmental programs require different levels of Bmp signaling during mouse retinal development. *Development*. 2005;132:913–923.
16. Dharmarajan S, Gurel Z, Wang S, Sorenson CM, Sheibani N, Belecky-Adams TL. Bone morphogenetic protein 7 regulates reactive gliosis in retinal astrocytes and Müller glia. *Mol Vis*. 2014;20:1085–1108.
17. Hrabé de Angelis M, Flaswinkel H, Fuchs H, et al. Genome-wide, large-scale production of mutant mice by ENU mutagenesis. *Nat Genet*. 2000;25:444–447.
18. Ehling UH, Charles DJ, Favor J, et al. Induction of gene mutations in mice: the multiple endpoint approach. *Mutat Res*. 1985;150:393–401.
19. Aigner B, Rathkolb B, Klempt M, et al. Generation of N-ethyl-N-nitrosourea-induced mouse mutants with deviations in hematological parameters. *Mamm Genome*. 2011;22:495–505.
20. Fuchs H, Schughart K, Wolf E, Balling R, Hrabé de Angelis M. Screening for dysmorphological abnormalities—a powerful tool to isolate new mouse mutants. *Mamm Genome*. 2000;11:528–530.
21. Klaften M, Hrabé de Angelis M. ARTS: a web-based tool for the set-up of high-throughput genome-wide mapping panels for the SNP genotyping of mouse mutants. *Nucl Acids Res*. 2005;33:W496–W500.
22. Gailus-Durner V, Fuchs H, Becker L, et al. Introducing the German Mouse Clinic: open access platform for standardized phenotyping. *Nat Methods*. 2005;2:403–404.
23. Gailus-Durner V, Fuchs H, Adler T, et al. Systemic first-line phenotyping. *Methods Mol Biol*. 2009;530:463–509.
24. Puk O, Hrabé de Angelis M, Graw J. Longitudinal fundus and retinal studies with SD-OCT: a comparison of five mouse inbred strains. *Mamm Genome*. 2013;24:198–205.
25. Prusky GT, Alam NM, Beekman S, Douglas RM. Rapid quantification of adult and developing mouse spatial vision using a virtual optomotor system. *Invest Ophthalmol Vis Sci*. 2004;45:4611–4616.
26. Heiduschka P, Schnichels S, Fuhrmann N, et al. Electrophysiological and histologic assessment of retinal ganglion cell fate in a mouse model for *OPA1*-associated autosomal dominant optic atrophy. *Invest Ophthalmol Vis Sci*. 2010;51:1424–1431.
27. Harazny J, Scholz M, Buder T, Lausen B, Kremers J. Electrophysiological deficits in the retina of the DBA/2J mouse. *Doc Ophthalmol*. 2009;119:181–197.
28. Gerding WM, Schreiber S, Schulte-Middelmann T, et al. *Ccdc66* null mutation causes retinal degeneration and dysfunction. *Hum Mol Genet*. 2011;20:3620–3631.
29. Atorf J, Scholz M, Garreis F, et al. Functional protective effects of long-term memantine treatment in the DBA/2J mouse. *Doc Ophthalmol*. 2013;126:221–232.
30. Yan X, Sabrautzki S, Horsch M, et al. Peroxidasin is essential for eye development in the mouse. *Hum Mol Genet*. 2014;23:5597–5614.
31. Pittler SJ, Zhang Y, Chen S, et al. Functional analysis of the rod photoreceptor cGMP phosphodiesterase alpha-subunit gene promoter: Nrl and Crx are required for full transcriptional activity. *J Biol Chem*. 2004;279:19800–19807.
32. Mali RS, Zhang X, Hoerauf W, et al. FIZ1 is expressed during photoreceptor maturation, and synergizes with NRL and CRX at rod-specific promoters in vitro. *Exp Eye Res*. 2007;84:349–360.
33. Greferath U, Grünert U, Wässle H. Rod bipolar cells in the mammalian retina show protein kinase C-like immunoreactivity. *J Comp Neurol*. 1990;301:433–442.
34. Beby F, Lamonerie T. The homeobox gene *Otx2* in development and disease. *Exp Eye Res*. 2013;111:9–16.
35. Haverkamp S, Wässle H. Immunocytochemical analysis of the mouse retina. *J Comp Neurol*. 2000;424:1–23.
36. Takahashi H, Kanesaki H, Igarashi T, et al. Reactive gliosis of astrocytes and Müller glial cells in retina of POMGnT1-deficient mice. *Mol Cell Neurosci*. 2011;47:119–130.
37. Sarkar A, Hochedlinger K. The Sox family of transcription factors: versatile regulators of stem and progenitor cell fate. *Cell Stem Cell*. 2013;12:15–30.
38. Soukkarieh C, Agius E, Soula C, Cochard P. Pax2 regulates neuronal-glial cell fate choice in the embryonic optic nerve. *Dev Biol*. 2007;303: 800–813.
39. Philips GT, Stair CN, Young Lee H, et al. Precocious retinal neurons: Pax6 controls timing of differentiation and determination of cell type. *Dev Biol*. 2005;279:308–321.
40. Sansom SN, Griffiths DS, Faedo A, et al. The level of the transcription factor Pax6 is essential for controlling the balance between neural stem cell self-renewal and neurogenesis. *PLoS Genet*. 2009;5:e1000511.
41. Pichaud F, Desplan C. *Pax* genes and eye organogenesis. *Curr Opin Genet Dev*. 2002;12:430–434.
42. Wall PB, Traboulsi EI. Congenital abnormalities of the optic nerve: from gene mutation to clinical expression. *Curr Neurol Neurosci Rep*. 2013;13:363.

Investigative Ophthalmology & Visual Science

43. Xiang M Requirement for Brn-3b in early differentiation of postmitotic retinal ganglion cell precursors. *Dev Biol*. 1998;197:155–169.
44. Lee J, Choi SH, Kim YB, et al. Defined Conditions for Differentiation of Functional Retinal Ganglion Cells From Human Pluripotent Stem Cells. *Invest Ophthalmol Vis Sci*. 2018;59:3531–3542.
45. Pekny M, Wilhelmsson U, Pekna M. The dual role of astrocyte activation and reactive gliosis. *Neurosci Lett*. 2014;565:30–38.
46. Dutton GN. Congenital disorders of the optic nerve: excavations and hypoplasia. *Eye*. 2004;18:1038–1048.
47. Gregory-Evans CY, Williams MJ, Halford S, Gregory-Evans K. Ocular coloboma: a reassessment in the age of molecular neuroscience. *J Med Genet*. 2004;41:881–891.
48. Ninomiya H, Kuno H, Inagaki S. Vascular changes associated with chorioretinal and optic nerve colobomas in rats (Crj: CD(SD), IGS). *Vet Ophthalmol*. 2005;8:319–323.
49. Gopal L. Pattern of blood vessels in eyes with coloboma. *Ind J Ophthalmol*. 2013;61:743–748.
50. Chida A, Shintani M, Nakayama T, et al. Missense mutations of the *BMPR1B* (*ALK6*) gene in childhood idiopatic pulmonary arterial hypertension. *Circ J*. 2012;76:1501–1508.
51. Lam CF, Peterson TE, Croatt AJ, Nath KA, Katusic ZS. Functional adaptation and remodeling of pulmonary artery in flow-induced pulmonary hypertension. *Am J Physiol Heart Circ Physiol*. 2005;289:2334–2345.
52. Tagami M, Honda S, Morioka I, Matsuo M, Negi A. Bilateral optic disc anomalies associated with *PAX2* mutation in a case of Potter sequence. *Case Report Ophthalmol*. 2010;1:94–98.
53. Favor J, Sandulache R, Neuhäuser-Klaus A, et al. The mouse *Pax2*^{1Neu} mutation is identical to a human *PAX2* mutation in a family with renal-coloboma syndrome and results in developmental defects of the brain, ear, eye, and kidney. *Proc Natl Acad Sci USA*. 1996;93:13870–13875.
54. Alur RP, Vijayasarathy C, Brown JD, et al. Papillorenal syndrome-causing missense mutations in PAX2/Pax2 result in hypomorphic alleles in mouse and human. *PLoS Genet*. 2010;6:e1000870.
55. Alur RP, Cox TA, Crawford MA, Gong X Brooks BP. Optic nerve axon number in mouse is regulated by *PAX2*. *J AAPOS*. 2008;12:117–121.
56. Viringipurampeer IA, Ferreira T, DeMaria S, et al. Pax2 regulates a fadd-dependent molecular switch that drives tissue fusion during eye development. *Hum Mol Genet*. 2012;21:2357–69.
57. Sehgal R, Sheibani N, Rhodes SJ, Belecky Adams TL. BMP7 and SHH regulate *Pax2* in mouse retinal astrocytes by relieving TLX repression. *Dev Biol*. 2009;332:429–443.
58. Miyawaki T, Uemura A, Dezawa M, et al. Tlx, an orphan nuclear receptor, regulates cell numbers and astrocyte development in the developing retina. *J Neurosci*. 2004;24:8124–8134.
59. Hsieh YW, Yang XJ. Dynamic Pax6 expression during the neurogenic cell cycle influences proliferation and cell fate choices of retinal progenitors. *Neural Dev*. 2009;4:32.
60. Buffo A, Rite I, Tripathi P, et al. Origin and progeny of reactive gliosis: a source of multipotent cells in the injured brain. *Proc Natl Acad Sci USA*. 2009;105:3581–3586.
61. Feigenson K, Reid M, See J, Crenshaw III EB, Grinspan JB. Canonical Wnt signalling requires the BMP pathway to inhibit oligodendrocyte maturation. *ASN Neuro*. 2011;3:e00061.
62. Sahni V, Mukhopadhyay A, Tysseling V, et al. BMPR1a and BMPR1b signaling exert opposing effects on gliosis after spinal cord injury. *J Neurosci*. 2010;30:1839–1855.
63. See J, Mamontov P, Ahn K, et al. BMP signaling mutant mice exhibit glial cell maturation defects. *Mol Cell Neurosci*. 2007;35:171–182.
64. Lee J, Son MJ, Woolard K, et al. Epigenetic-mediated dysfunction of the bone morphogenetic protein pathway inhibits differentiation of glioblastoma-initiating cells. *Cancer Cell*. 2008;13:69–80.
65. Dharmarajan S, Fisk DL, Sorenson CM, Sheibani N, Belecky-Adams TL. Microglia activation is essential for BMP7-mediated retinal reactive gliosis. *J Neuroinflammation*. 2017;14:76.
66. Yi SE, Daluiski A, Pederson R, Rosen V, Lyons KM. The type I BMP receptor BMPRIB is required for chondrogenesis in the mouse limb. *Development*. 2010;127:621–630.

Investigative Ophthalmology & Visual Science

Supplementary Materials

Mutation in *Bmpr1b* Leads to Optic Disc Coloboma and Ventral Retinal Gliosis in Mice

Xiaohe Yan[2,10*], Jenny Atorf[3ж], David Ramos[4], Frank Thiele[5&], Susanne Weber[1], Claudia Dalke[1,7], Minxuan Sun[1,7ɹ], Oliver Puk[1,7$], Dian Michel[5#], Helmut Fuchs[5,7], Matthias Klaften[5§], Gerhard K.H. Przemeck[5], Sibylle Sabrautzki[5X], Jack Favor[6,7], Jesús Ruberte[4], Jan Kremers[3], GMC-Consortium[+], Martin Hrabě de Angelis[5,7,8,9], Jochen Graw[1,7]

[1]Institutes of Developmental Genetics, [5]Experimental Genetics, and [6]Human Genetics, and the [7]German Mouse Clinic, Helmholtz Zentrum München, Neuherberg, Germany;
[2]Shenzhen Key Laboratory of Ophthalmology, Shenzhen Eye Hospital, Jinan University, Shenzhen, China;
[3]Department of Ophthalmology, University Hospital Erlangen, Erlangen, Germany;
[4]Department of Animal Health and Anatomy, Center of Animal Biotechnology and Gene Therapy, Universitat Autònoma de Barcelona, Spain;
[8]Chair of Experimental Genetics, Faculty of Life and Food Sciences Weihenstephan, Technische Universität München, Freising-Weihenstephan, Germany;
[9]German Center for Diabetes Research (DZD), Neuherberg, Germany;
[10]School of Optometry, Shenzhen University, Shenzhen, China.

[ж]present address: Municipal Eye Hospital, Karlsruhe, Germany;
[&]present address: Helmholtz Zentrum München, Institute of Virology, München, and Institute of Virology, Technical University Munich, München, Germany;
[ɹ]present address: Jiangsu Key Lab of Medical optics, Suzhou Institute of Biomedical Engineering and Technology, Chinese Academy of Sciences, Suzhou, China;
[$]present address: Practice of Human Genetics, Tübingen, Germany;
[#]present address: Freie Universität Berlin, Dahlem Research School, Berlin, Germany;
[§]present address: amcure GmbH, Eggenstein-Leopoldshafen, Germany.
[X]present address: Research Unit Comparative Medizin, Helmholtz Zentrum München, Neuherberg, Germany
[+]A full list of consortium members appears in the appendix.

Comprehensive phenotyping screening at the German Mouse Clinic (GMC)

Comprehensive phenotyping was performed at the German Mouse Clinic (GMC). In the morphological investigation via visual inspection and X-ray analysis, we observed shortened and distorted limbs in the homozygous mutants. In the dual-energy X-ray absorptiometry (DXA), all bone parameters and almost all body parameters were changed in mutants. *ALI030* mutants showed several differences in energy metabolism parameters with decreased body mass and complex effects on energy assimilation. Moreover, *ALI030* mutants showed a sex-dependent change in locomotor activity and anxiety behavior in the Open Field, and a prepulse inhibition deficit, occurring mainly in male mice.

The results of all screens are summarized in Table S1; the detailed results of the eye phenotypic analysis of the mice are described in the main text.

Skeletal changes: In the morphological investigation via visual inspection and X-ray analysis, we confirmed shortened and distorted limbs in the mutants. In the dual-energy X-ray absorptiometry (DXA), all bone parameters and almost all body parameters were changed in the mutants. Heterozygous mutants did not show any obvious anomalies, whereas homozygous mutant mice were smaller (Fig. S2a) and presented with shortened, distorted limbs and syndactyly in the fore- and hind-limbs (Fig. S2b). Therefore, this mouse line was referred to as abnormal limb #030 (*ALI030*) according to the internal lab code.

Eye abnormalities: Significant genotype-specific differences between wild-type control and mutant ALI030 mice were detected by Ophthalmoscopy, Laser Interference Biometry and histological analysis, namely larger axial eye length and en-larged optic disc.

Metabolic changes: Interestingly, alkaline phosphatase activity was not changed in the mutants compared to the wild-type mice. Therefore, bone turnover does not seem to be affected although bone morphology and density were changed. We detected reduced blood lipid and protein values in the mutant animals, suggesting a state of negative energy balance or impaired liver function. *ALI030* mutants showed several differences in energy metabolism parameters with decreased body mass and complex effects on energy assimilation.

Alterations in Behavior: ALI030 mutants show a sex-dependent increase in locomotor activity and a decreased anxiety behavior in the Open Field together with deficit in the prepulse inhibition, both occurring mainly in male mice. These changes suggest central effects of the mutation, the neurobiology of which remains to be determined.

Immunology: The analysis of ALI030 mutant mice in the primary Immunology Screen revealed no statistically significant differences in the frequencies of main leukocyte populations between mutant mice compared to controls. In male mutant mice, a lower frequency of CD62L-coexpressing cells within the T-cell cluster has been found. Furthermore, a very minor reduction in the expression of CD44 on CD4 T-cells in female mice has been found. The analysis of the blood plasma did not

show statistically different levels of antibodies in ALI030 mutant mice, but extraordinary high antibody levels in females.

Pathology: The ALI030 mutant mice showed a congenital anomaly with shortened, distorted front and hind limbs (100% penetrance). There were no obvious morphological changes affecting the endocrine organs. In the screens concerning neurology, allergy, steroid metabolism, cardiovascular system or lung function, no genotype-specific differences were observed.

Table S1: Phenotyping overview of the homozygous Ali30 mutant mice

Screen	Test	Description of the phenotype	Number of animals tested (Male mutants/M controls//Female mutants/F controls)
Dysmorphology	Anatomical observation BMD BMC Bone content Body weight Fat mass Click box (hearing)	Shortened and distorted limbs and digits decreased decreased decreased decreased decreased No	10/10//10/10
Cardiovascular	Blood pressure Heart weight ANP ECG or Echo	No No No No	10/10//9/10
Energy Metabolism	Calorimetry	Complex effects on energy assimilation	7/7//7/7
Clinical Chemistry	Simplified IpGTT Clinical chemical analysis Hematology	No Reduced blood lipid and protein No	10/10//10/10
Eye	Eye size Ophthalmoscopy Slit lamp	Increased Enlarged optic disc No	7/7//7/7 9/11//11/9 9/11//11/9
Lung function	Plethysmography	No	6/6//6/6
Behavior	Open field PPI	In males: increased locomotion, decreased anxiety PPI deficit in males	11/8//9/10
Neurology	Modified SHIRPA (Grip strengthRotarod)	No (Not tested due to limb malformation)	11/9//9/10
Immunology & Allergy	FCM analysis of PBCs IgG/IgM/IgAconc IgE conc	No No	5/6//9/10 10/10//10/10
Steroid Metabolism	DHEA Testosterone	No No	11/9//9/10
Pathology	Macro- and microscopic analysis	Limb anomalies No obvious anomalies in theendocrine systems	3/3//3/3

Abbreviations:
ANP, atrial natriuretic peptide;
BMC, bone mineral content
BMD, bone mineral density
DXA, dual-energy X-ray absorptiometry;

FCM, flow cytometry
ECG, electrocardiography;
DHEA, dehydroepiandrosterone;
PBCs, peripheral blood cells;
PPI, prepulse inhibition

Table S2

a. Primary antibodies

Target protein	Species	Dilution	Catalog number	Company
BrdU	Rat	1:500	OBT0030CX	AbD Serotec, Germany
BRN3	Goat	1:100	Sc-6026	Santa Cruz, Germany
Calretinin	Rabbit	1:1000	7699/3H	Swant, Switzerland
Collagen IV	Rabbit	1:200	AB756P	Millipore, Germany
Glutamine Synthetase	Mouse	1:200	BD 610517	BD Biosciences, Germany
Neurofilament 2H3	Mouse	1:100	None	Developmental Studies Hybridoma Bank, U.S
Neurofilament 200	Rabbit	1:500	N4142	Santa Cruz, Germany
OTX2	Rabbit	1:200	a gift from Dr. Antonio Simeone, Institute of Genetics and Biophysics, CNR, Napoli, Italy	
PAX2	Rabbit	1:200	2549-1	Epitomics, Germany
PAX6	Rabbit	1:400	PRB-278P	Chemicon, Germany
PDE6b	Rabbit	1:500	PA1-722	Thermo Scientific, Germany
PKC-α	Mouse	1:500	Ab1723	Abcam, Germany
PROX1	Rabbit	1:1000	AB 5475	Millipore, Germany
SOX2	Goat	1:500	sc-17320	Santa Cruz, Germany

b. Secondary antibodies

Name	Species	Dilution	Catalog No.	Company
Alexa Fluor ® 488	Anti-Rabbit	1:250	A21206	Invitrogen, Germany
Alexa Fluor ® 488	Anti-Rat	1:250	A21208	Invitrogen, Germany
Cy3	Anti-Goat	1:250	705-165-147	Dianova, Germany
Cy3	Anti-Rat	1:250	712-165-153	Dianova, Germany
Cy5	Anti-Mouse	1:250	715-175-150	Jackson immuno, Germany

Figure S1

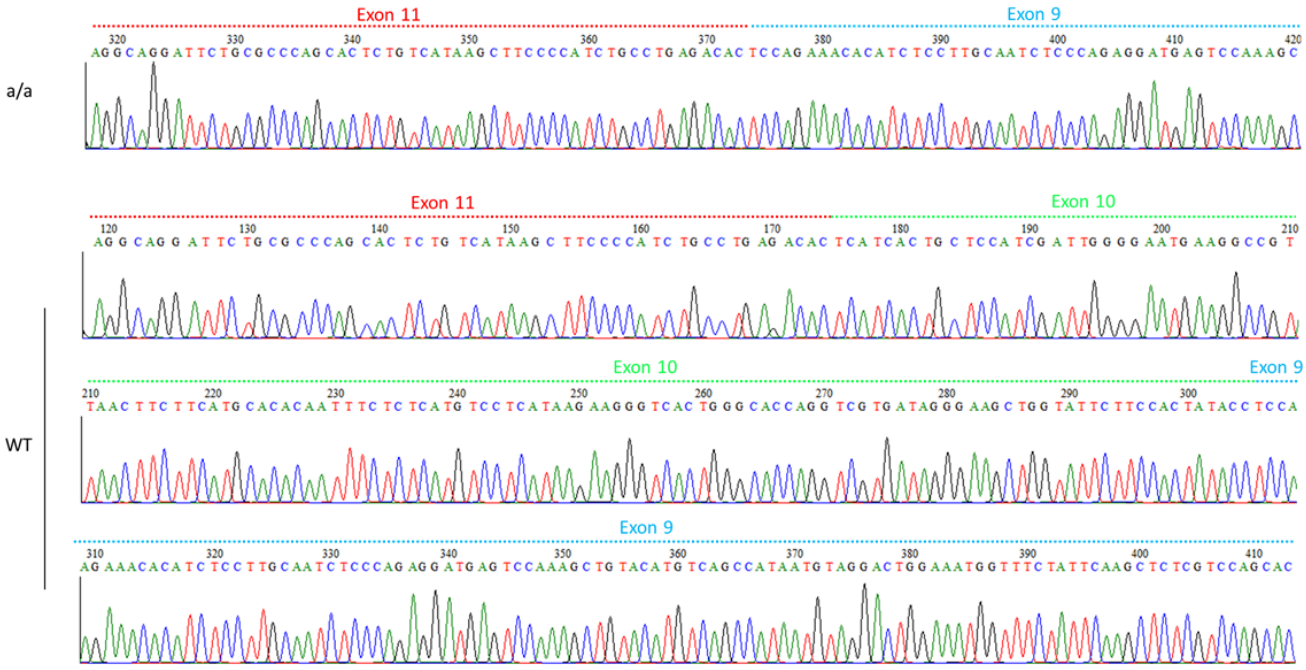

Figure S2.

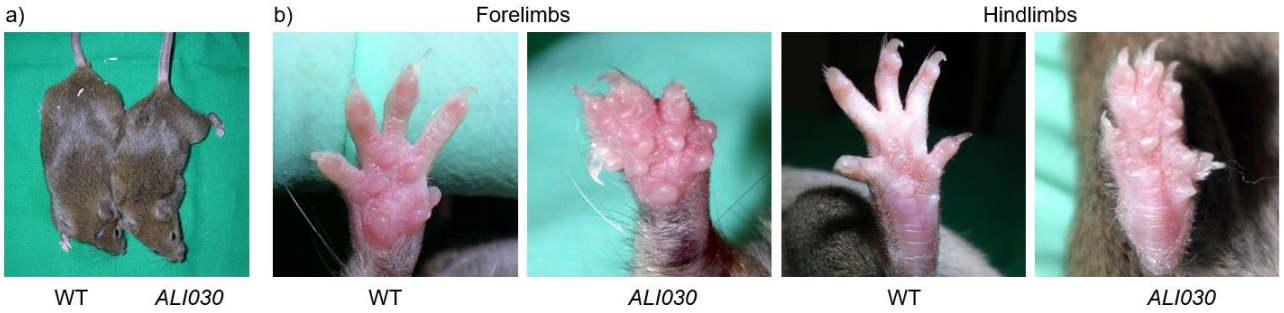

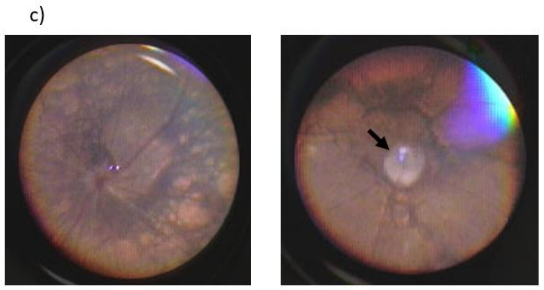

Figure S3.

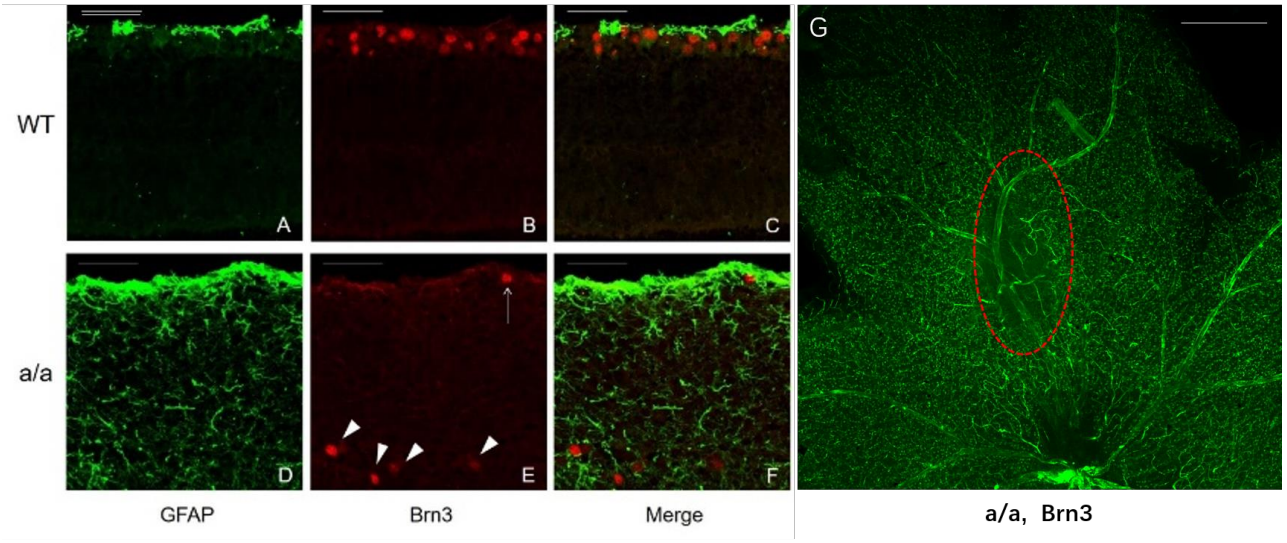

Supplemental Figure Legends

Fig. S1: **Sequence analysis of the *ALI030* mutant mouse.**

Sequence analysis of *Bmpr1b* cDNA demonstrates mis-splicing of exon 10 in *ALI030* mutants. Exon 10 is skipped in homozygous mutants compared to wild types.

Fig. S2: **Phenotype of the *ALI030* mutant mouse.**

a) At the age of 12 weeks, homozygous mutant mice (*ALI030*) are smaller than wild-type mice (WT).

b) Syndactylism of the forelimbs and hindlimbs.

c) Retinal fundus photo of a wild-type C3HeB/FeJ (C3H) mouse and a *ALI030* mutant showing an enlarged optic disc (arrow).

Fig. S3: **Retinal ganglion cells of the *ALI030* mutant mouse.**

At the age of 8 weeks, retinal ganglion cells are almost absent in the ventral gliosis retina of the homozygous mutant mice (*a/a*) (A-C) compared to the wild-type mice (WT) (D-F). Flat-mount retina immunofluorescence against Brn3a also showed absent retinal ganglion cells in the ventral gliosis area (G, red circle) of the mutants. Scale bar: 100 μm.

APPENDIX X:

[+]German Mouse Clinic, Helmholtz Zentrum München, German Research Center for Environmental Health GmbH, Neuherberg, Germany

Antonio Aguilar-Pimentel[1]

Markus Ollert[3]

Holger Schulz[1,4]

Lore Becker[1,5]

Thomas Klopstock [5,14,15,18,19]

Thure Adler[1]

Dirk H. Busch [2]

Anja Schrewe[1]

Hugo A. Katus[6]

Lillian Garrett[1,8]

Sabine M. Hölter [1,8]

Wolfgang Wurst [8,13,14,15]

Wolfgang Hans[1]

Jan Rozman [1,17]

Martin Klingenspor[9,10]

Julia Calzada-Wack[1,7]

Birgit Rathkolb [1,11,17]

Eckhard Wolf [11]

Cornelia Prehn[12]

Jerzy Adamkski[12,13,17]

Manuela Östereicher[1]

Gregor Miller[1]

Christoph Lengger[1]

Holger Maier[1]

Claudia Stoeger[1]

Stefanie Leuchtenberger[1]

Valérie Gailus-Durner [1]

Helmut Fuchs [1]

Martin Hrabě de Angelis [1,16,17]

1 German Mouse Clinic, Institute of Experimental Genetics, Helmholtz Zentrum München, German Research Center for Environmental Health GmbH, Ingolstädter Landstrasse 1, 85764 Neuherberg, Germany

2 Institute for Medical Microbiology, Immunology and Hygiene, Technical University of Munich, Trogerstrasse 30, 81675 Munich, Germany

3 Department of Infection and Immunity, Luxembourg Institute of Health, Esch-sur- Alzette, Luxembourg, and Department of Dermatology and Allergy Center, Odense Research Center for Anaphylaxis, University of Southern Denmark, Odense, Denmark

4 Institute of Epidemiology, Helmholtz Zentrum München, German Research Center for Environmental Health GmbH, Ingolstädter Landstraße 1, 85764 Neuherberg, Germany and Member of the German Center for Lung Research

5 Department of Neurology, Friedrich-Baur-Institut, Ludwig-Maximilians-Universität München, Ziemssenstrasse 1a, 80336 Munich, Germany

6 Department of Cardiology, University of Heidelberg, Im Neuenheimer Feld 410, 69120 Heidelberg, Germany

7 Institute of Pathology, Helmholtz Zentrum München, German Research Center for Environmental Health GmbH, Ingolstädter Landstrasse 1, 85764 Neuherberg, Germany

8 Institute of Developmental Genetics, Helmholtz Zentrum München, German Research Center for Environmental Health GmbH, Ingolstädter Landstrasse 1, 85764 Neuherberg, Germany

9 Chair of Molecular Nutritional Medicine, Technical University Munich, EKFZ – Else Kröner Fresenius Center for Nutritional Medicine, Gregor-Mendel-Str. 2, 85350 Freising-Weihenstephan, Germany

10 ZIEL – Institute for Food and Health, Technical University Munich, Gregor- Mendel-Str. 2, 85350 Freising-Weihenstephan, Germany

11 Ludwig-Maximilians-Universität München, Gene Center, Institute of Molecular Animal Breeding and Biotechnology, Feodor-Lynen Strasse 25, 81377 Munich, Germany

12 Molekulare Endokrinologie und Metabolismus, Helmholtz Zentrum München, German Research Center for Environmental Health GmbH, Ingolstädter Landstrasse 1, 85764 Neuherberg, Germany

13 Chair of Developmental Genetics, Center of Life and Food Sciences Weihenstephan, Technische Universität München, Ingolstädter Landstrasse 1, 85764 Neuherberg, Germany

14 Deutsches Institut für Neurodegenerative Erkrankungen (DZNE) Site Munich, Schillerstrasse 44, 80336 Munich, Germany

15 Munich Cluster for Systems Neurology (SyNergy), Adolf-Butenandt-Institut, Ludwig-Maximilians-Universität München, Schillerstrasse 44, 80336 Munich, Germany

16 Chair of Experimental Genetics, Center of Life and Food Sciences Weihenstephan, Technische Universität München, 85354 Freising-Weihenstephan, Germany

17 Member of German Center for Diabetes Research (DZD), Ingolstädter Landstraße 1, 85764 Neuherberg, Germany

18 German Network for Mitochondrial Disorders (mitoNET)

19 German Center for Vertigo and Balance Disorders, Munich, Germany